การจำลองการขนส่งอนุภาคทรงกลมผ่านไฮโดรเจลและแถวไฟเบอร์ขนานเพื่อการประยุกต์กับการกรองผ่านโกลเมอร์รูลัสในคนปกติและผู้ป่วยโรคไต

นายนำพงศ์ บุณยรัตพันธุ์

จุฬาลงกรณ์มหาวิทยาลัย
Chulalongkorn University

บทคัดย่อและแฟ้มข้อมูลฉบับเต็มของวิทยานิพนธ์ตั้งแต่ปีการศึกษา 2554 ที่ให้บริการในคลังปัญญาจุฬาฯ (CUIR)
เป็นแฟ้มข้อมูลของนิสิตเจ้าของวิทยานิพนธ์ ที่ส่งผ่านทางบัณฑิตวิทยาลัย
The abstract and full text of theses from the academic year 2011 in Chulalongkorn University Intellectual Repository (CUIR)
are the thesis authors' files submitted through the University Graduate School.

วิทยานิพนธ์นี้เป็นส่วนหนึ่งของการศึกษาตามหลักสูตรปริญญาวิทยาศาสตรมหาบัณฑิต
สาขาวิชาฟิสิกส์ ภาควิชาฟิสิกส์
คณะวิทยาศาสตร์ จุฬาลงกรณ์มหาวิทยาลัย
ปีการศึกษา 2558
ลิขสิทธิ์ของจุฬาลงกรณ์มหาวิทยาลัย

SIMULATION OF TRANSPORT OF SPHERICAL PARTICLES THROUGH HYDROGEL AND ROW OF PARALLEL FIBERS FOR APPLICATIONS IN GLOMERULAR FILTRATION IN NORMAL AND NEPHROTIC HUMANS

Mr. Numpong Punyaratabandhu

จุฬาลงกรณ์มหาวิทยาลัย
Chulalongkorn University

A Thesis Submitted in Partial Fulfillment of the Requirements
for the Degree of Master of Science Program in Physics
Department of Physics
Faculty of Science
Chulalongkorn University
Academic Year 2015
Copyright of Chulalongkorn University

Thesis Title	SIMULATION OF TRANSPORT OF SPHERICAL PARTICLES THROUGH HYDROGEL AND ROW OF PARALLEL FIBERS FOR APPLICATIONS IN GLOMERULAR FILTRATION IN NORMAL AND NEPHROTIC HUMANS
By	Mr. Numpong Punyaratabandhu
Field of Study	Physics
Thesis Advisor	Panadda Dechadilok, Ph.D.

Accepted by the Faculty of Science, Chulalongkorn University in Partial Fulfillment of the Requirements for the Master's Degree

.....Dean of the Faculty of Science
(Associate ProfessorPolkit Sangvanich, Ph.D.)

THESIS COMMITTEE

.....Chairman
(Assistant ProfessorRattachat Mongkolnavin, Ph.D.)
.....Thesis Advisor
(Panadda Dechadilok, Ph.D.)
.....Examiner
(Sathon Vijarnwannaluk, Ph.D.)
.....External Examiner
(Panwong Kuntanawat, Ph.D.)

จุฬาลงกรณ์มหาวิทยาลัย
Chulalongkorn University

นำพงศ์ บุณยรัตพันธุ์ : การจำลองการขนส่งอนุภาคทรงกลมผ่านไฮโดรเจลและแถวไฟเบอร์ขนานเพื่อการประยุกต์กับการกรองผ่านโกลเมอร์รูลัสในคนปกติและผู้ป่วยโรคไต (SIMULATION OF TRANSPORT OF SPHERICAL PARTICLES THROUGH HYDROGEL AND ROW OF PARALLEL FIBERS FOR APPLICATIONS IN GLOMERULAR FILTRATION IN NORMAL AND NEPHROTIC HUMANS) อ.ที่ปรึกษาวิทยานิพนธ์หลัก: อ. ดร.ปนัดดา เดชาดิลก, 80 หน้า.

ไตเป็นอวัยวะที่ทำหน้าที่กรองของไหลและตัวถูกละลายส่วนเกินรวมไปถึงของเสียจากกระบวนการเผาผลาญเพื่อรักษาองค์ประกอบและปริมาตรของเลือดให้อยู่ในระดับปกติ เราเชื่อกันว่าขั้นตอนแรกของการเกิดปัสสาวะของไตคือกระบวนการกรองเลือดผ่านผนังหลอดเลือดฝอยในโกลเมอร์รูลัสซึ่งประกอบด้วยเนื้อเยื่อ 3 ชั้น ได้แก่ ชั้นเซลล์เนื้อเยื่อบุโพรง. โกลเมอร์รูลาร์ เบสเมนต์ เมมเบรนและชั้นเซลล์เนื้อเยื่อบุผิว ในปัจจุบัน ถึงแม้ว่าจะมีการทดลองทางการแพทย์มากมายเกี่ยวกับการกรองเลือดผ่านโกลเมอร์รูลัส แต่ความเข้าใจในผลของสมบัติพื้นฐานของตัวถูกละลายและอันตรกิริยาระหว่างตัวถูกละลายกับโครงสร้างระดับนาโนที่มีต่อการกรองมหโมเลกุลและของไหลก็ยังคงไม่สมบูรณ์ วัตถุประสงค์ของการวิจัยที่นำเสนอในวิทยานิพนธ์นี้คือการศึกษาผลของขนาดของอนุภาคและอันตรกิริยาระหว่างอนุภาคกับโครงสร้างระดับนาโนของเนื้อเยื่อทั้ง 3 ชั้นที่มีต่อทั้งการคัดกรองโดยใช้ขนาดของโกลเมอร์รูลัสและการซึมผ่านของของไหลโดยใช้การจำลองทางคณิตศาสตร์ ในงานวิทยานิพนธ์ชิ้นนี้แบบจำลองระดับจุลภาคที่ Edwards และ Deen เคยทำไว้ในปี 1999 จะถูกนำมาใช้ในงานวิทยานิพนธ์ชิ้นนี้ นอกเหนือจากบทบาทในการกีดขวางตัวถูกละลายของโกลเมอร์รูลาร์ เบสเมนต์ เมมเบรนและชั้นเซลล์เนื้อเยื่อบุผิวแล้ว ผลของชั้นเซลล์เนื้อเยื่อบุโพรงที่มีต่อเรื่องดังกล่าวก็จะถูกพิจารณาเพิ่มเข้าไปด้วยโกลเมอร์รูลาร์ เบสเมนต์ เมมเบรนจะถูกจำลองเป็นไฮโดรเจลที่ประกอบด้วยคอลลาเจนประเภทที่ 4 และไกลโคอะมิโนไกลแคน เราจะศึกษาบทบาทของเส้นใยทั้งสองชนิดที่มีต่อการแพร่ของตัวถูกละลายที่ถูกกีดขวางในชั้นดังกล่าวโดยใช้ทฤษฎีเกี่ยวกับการแพร่ในตัวกลางอันเต็มไปด้วยเส้นใยที่มีอยู่ เราพบว่าอันตรกิริยาเฉพาะไกลโคอะมิโนไกลแคนกับตัวถูกละลายเท่านั้นที่มีผลต่อแรงต้านและสภาพการแพร่ของตัวถูกละลาย ในทางกลับกัน เราจะศึกษาการพาของตัวถูกละลายที่ถูกกีดขวางด้วยทฤษฎีของตัวกลางแบบบริงค์แมนโดยใช้ค่าการซึมผ่านของดาร์ซีของโกลเมอร์รูลาร์ เบสเมนต์ เมมเบรน สำหรับชั้นเซลล์เนื้อเยื่อบุผิว เราจะมองสลิตไดอะเฟรมในชั้นเนื้อเยื่อดังกล่าวเป็นแถวไฟเบอร์ขนานที่มีขนาดของช่องว่างระหว่างไฟเบอร์ไม่สม่ำเสมอกันโดยเป็นไปตามการกระจายแบบแกมมาหรือแบบลอกนอร์มอล เราจะตั้งค่าเฉลี่ยของครึ่งหนึ่งของขนาดช่องว่างระหว่างไว้ที่ 12.10(ค่าที่ได้จากการสังเกตด้วยกล้องจุลทรรศน์อิเลกตรอนแบบส่องกราด), 22(ค่าที่ได้จากการสังเกตด้วยกล้องจุลทรรศน์แบบใช้ไอออนของฮีเลียม) และ 2 นาโนเมตร(ค่าที่ได้จาการสังเกตกล้องจุลทรรศน์อิเลกตรอนแบบส่องผ่านและเทคนิคอิเลกตรอน โทโมกราฟี) ส่วนชั้นเซลล์เนื้อเยื่อบุโพรงนั้นถูกจำลองเป็นแบบชั้นที่มีช่องซึ่งขนาดใหญ่กว่าตัวถูกละลายมากอันถูกปิดด้วยชั้นเยื่อหุ้มรอบนอกสุดที่อุดมไปด้วยไกลโคอะมิโนไกลแคน สมมติฐานสำหรับชั้นเนื้อเยื่อนี้คือเราสามารถละการคิดแรงต้านบนตัวถูกละลายอันเนื่องมาจากอันตรกิริยาระหว่างตัวถูกละลายกับผนังของช่องได้ และเฉพาะอันตรกิริยาระหว่างไกลโคอะมิโนไกลแคนกับตัวถูกละลายเท่านั้นที่ก่อให้เกิดการลดลงของสภาพการแพร่และการเปลี่ยนแปลงอัตราการพาของตัวถูกละลาย เราจะหาแฟคเตอร์บอกการกีดขวางการแพร่และการพาในชั้นเซลล์เนื้อเยื่อบุโพรงด้วยวิธีการเดียวกันกับที่ใช้กับโกลเมอร์รูลาร์ เบสเมนต์ เมมเบรน แต่เราจะคำนวณหาค่าบอกซึมผ่านของดาร์ซีของชั้นดังกล่าวโดยสมมติว่ามันเป็นเจลที่มีแถวของทรงกระบอกแบบไขว้ไปมา สัมประสิทธิ์การกรองแบบรวมที่คำนวณได้ภายใต้สมมติฐานข้างต้นสอดคล้องกับผลการทดลองที่ได้จากการตรวจปัสสาวะเมื่อร้อยละของปริมาตรของไกลโคอะมิโนไกลแคนในช่องของชั้นเซลล์เนื้อเยื่อบุโพรงเท่ากับ 7 โดยที่ไม่ขึ้นกับว่าค่าบอกการซึมผ่านของดาร์ซีของชั้นเซลล์เนื้อเยื่อบุโพรงเป็นเท่าใด ผลการคำนวณแสดงให้เห็นว่าชั้นเซลล์เนื้อเยื่อบุโพรงและโกลเมอร์รูลาร์ เบสเมนต์ เมมเบรนจะมีบทบาทสำคัญในการกีดขวางตัวถูกละลายของผนังหลอดเลือดฝอยในโกลเมอร์รูลัส โดยค่าบอกการซึมผ่านของแรงดันน้ำของโกลเมอร์รูลัสแบบรวมที่ได้จากการคำนวณจะมีค่าอยู่ในช่วงที่มีการรายงานไว้ในการกรองผ่านโกลเมอร์รูลัสของมนุษย์ สำหรับในกรณีของความผิดปกติที่เกิดขึ้นภายในไต การหายไปของสลิตไดอะเฟรมในชั้นเซลล์เนื้อเยื่อบุผิวจะทำให้สัมประสิทธิ์การกรองแบบรวมเปลี่ยนไปเพียงแค่เล็กน้อย แต่ถ้าชั้นเซลล์เนื้อเยื่อบุโพรงหายไปอีกชั้นหนึ่ง จะทำให้สัมประสิทธิ์การกรองโดยรวมเปลี่ยนไปมากถึงระดับขนาดหนึ่ง

ภาควิชา ฟิสิกส์ ลายมือชื่อนิสิต .....

สาขาวิชา ฟิสิกส์ ลายมือชื่อ อ.ที่ปรึกษาหลัก .....

ปีการศึกษา 2558

5772030723 : MAJOR PHYSICS
KEYWORDS: HYDROGEL / GLOMERULAR FILTRATION / SIEVING COEFFICIENT / FIBER / MATHEMATICAL MODEL / PHYSIOLOGY / NEPHROLOGY

NUMPONG PUNYARATABANDHU: SIMULATION OF TRANSPORT OF SPHERICAL PARTICLES THROUGH HYDROGEL AND ROW OF PARALLEL FIBERS FOR APPLICATIONS IN GLOMERULAR FILTRATION IN NORMAL AND NEPHROTIC HUMANS. ADVISOR: PANADDA DECHADILOK, Ph.D., 80 pp.

The renal main function is to remove excess fluid and solutes as well as metabolic waste to keep the normal blood volume and composition. It is believed that the first step of renal urine formation in kidney is blood ultrafiltration through glomerular capillary wall consisting of three cellular layers: the endothelium, the glomerular basement membrane (GBM) and the epithelium. The objective of the work presented in this thesis is to investigate how particle sizes and particle interaction with the nanostructure of the three layers affect glomerular size-selectivity and fluid permeability through the glomerular barrier using a mathematical simulation. The ultrastructural model, developed by Edwards and Deen (1999) is employed but with the effect of the endothelial cell layer on solute restriction included in addition to the contributions of the epithelial cell layer and the GBM. In this work, the GBM was modeled as a hydrogel consisting of type IV collagen and glycosaminoglycan (GAG). The contribution of two fibers to hindered diffusion of solutes in GBM was investigated using existing theory regarding diffusion in fibrous media. It is found that only the GAG-solute interaction had an effect on drag and solute diffusivity due to its much higher number in the GBM. The reduced diffusivity in the GAG-filled endothelium fenestrae was calculated the same way. Convective hindrance factor in the GBM was determined by employing the theory of Brinkman medium using its Darcy permeability. The slit diaphragm in the epithelial cell layer was modeled as row of parallel fibers with non-uniform spacing between adjacent fibers following the log-normal distribution. Mean values of half of fiber spacing were set at 12.10 (from scanning electron microscopy observation), 22 nm (from helium ion microscopy) and 2 nm (from transmitting electron microscopy observation and electron tomography). Endothelial cell layer was modeled as a layer having fenestrae that were much larger than solute sizes and filled with GAG-riched glycocalyx. The assumption for this layer was that the drag on solute due to solute-fenestrae wall interaction can be negligible, and only GAG-solute interaction in fenestrae caused diffusivity reduction and change in convection rate of solutes. Diffusive and convective hindrance factor in endothelium were completed in the same way as those in the GBM, but its Darcy permeability was calculated using the Amsden expression by assuming that it was gel with random array of cylinders. The obtained total sieving coefficient calculated under the assumption above agreed with experimental data from in vivo urinalysis, and the calculated hydraulic permeability falls within the range estimated from human glomerular filtration rate. The calculated results showed that the endothelial cell layer and the GBM significantly contributed to solute and fluid restriction of glomerular barrier. The absence of GAGs that filled the endothelial fenestrae can cause more than an order of magnitude increase in total sieving coefficient, whereas the contribution of the epithelial slit to glomerular size-selectivity is likely to be smaller than previously believed.

Department: Physics
Field of Study: Physics
Academic Year: 2015

Student's Signature .....
Advisor's Signature .....

ACKNOWLEDGEMENTS

After a long time, my thesis is finally completed. First, I would like to express my deepest gratitude to my advisor, Dr. Panadda Dechadilok, for her suggestions, keen interest and encouragement as well as for valuable guidance in dealing with simulation work.

I also would like to thank Asst. Prof. Dr. Rattachat Mongkolnavin, Dr. Sathon Vijarnwannaluk and Dr. Panwong Kuntanawat for taking the time from their busy schedules to be on my thesis committee. Their comments on this thesis are also greatly appreciated. I also would like to express my gratitude to Asst. Prof. Dr. Rattachat Mongkolnavin for his kindness in suggesting a utilization of electron microscopy observation of glomerular epithelial slit structure, and Assoc. Prof. Dr. Pisut Katavetin for his suggestion in including effects of type IV collagen and glycoaminoglycan to explain solute transport in the GBM instead of employing an effective fiber radius as previously planned.

I would like to express my gratitude to my family and my friends for their love and support. In addition, I would like to thank Mrs. Kularb Pimsuwan and Miss Varina Supakosol for their helpfulness and assistance.

Financial supports from The His Royal Highness Crown Prince Maha Vajiralongkorn Scholarship from the Graduate School, Chulalongkorn University to commemorate the 72nd anniversary of his Majesty King Bhumibala Aduladeja and The 90th Anniversary Chulalongkorn University Fund (Ratchadaphiseksomphot Endowment Fund) and Thai Research Fund (TRF) are gratefully acknowledged.

CONTENTS

Page

Page

จุฬาลงกรณ์มหาวิทยาลัย
Chulalongkorn University

List of Figures

List of Tables

จุฬาลงกรณ์มหาวิทยาลัย
Chulalongkorn University

Chapter 1
Introduction

1.1 Background and motivation

The main function of kidney is to filter blood to remove excess fluid and solutes as well as metabolic waste, keeping the blood volume and composition constant. Blood ultrafiltration through glomerular capillaries is believed to be the first step of renal urine formation in kidney, where fluid and solutes are transported from the blood stream in the capillary lumen through the glomerular capillary wall into primary urine in Bowman's capsule in the glomerulus as shown schematically in Fig. 1.1. The mammalian glomerular capillary has a unique structure consisting of several cellular layers as shown in the image from electron microscopy (Fig. 1.2). The filtrated fluid and solutes pass through the fenestrae of the endothelial cell layers, across the glomerular basement membrane (GBM), and through the slit diaphragm connecting the foot processes of the epithelial cells. Abnormality of glomerular capillary wall was found in patients with renal diseases such as membranous nephropathy and nephrotic Finnish syndrome where proteinuria (excess amounts of protein in urine) and changes in glomerular filtration rate (GFR) were observed.

There exist many medical experiments regarding glomerular blood filtration, including water transport and macromolecules selectivity of the glomerular capillary wall. It is known that the glomerular barrier allows fluid as well as small and medium-sized solutes to be filtrated into primary urine but hinders larger macromolecules such as albumin and IgG. However, effects of solute basic properties and solute-nanostructure interaction on fluid and macromolecules filtration are not completely understood. The work presented in this thesis aims at investigating the effects of particle sizes, and particle interaction with the nanostructure of each layers on both glomerular size-selectivity and fluid permeability using a mathematical simulation.

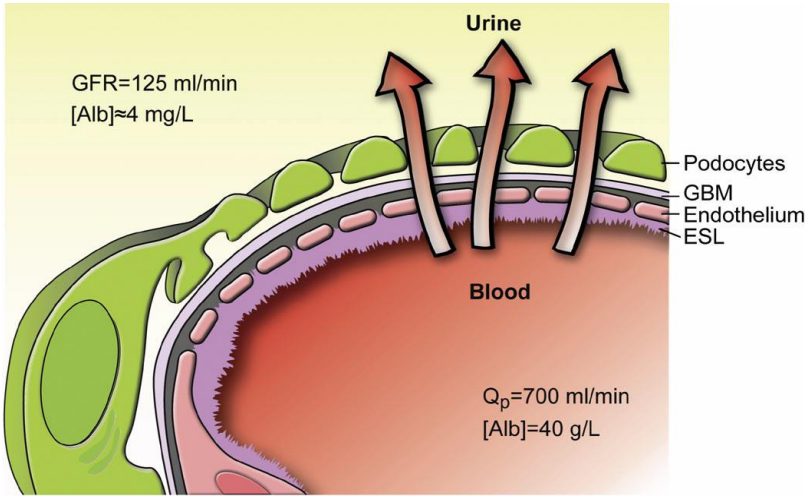

Figure 2.1 Schematic drawing of the glomerular barrier(Haraldsson et al., 2008). Arrows indicate the direction of fluid flow across the glomerular barrier from the capillary lumen into primary urine in the Bowman's capsule.

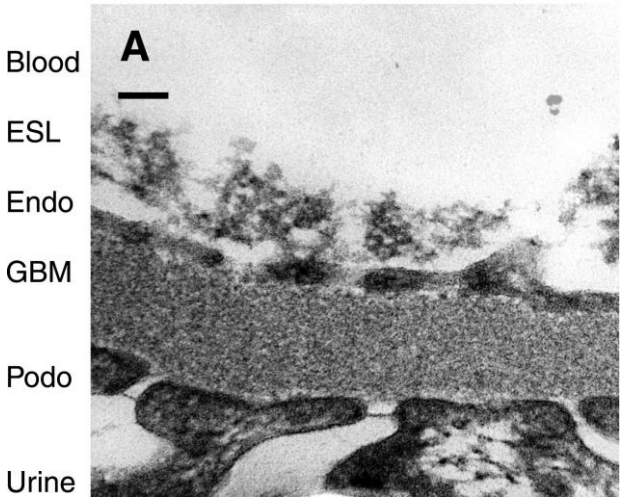

Figure 1.2 Electron microcraphs showing the glomerular capillary wall with the capillary lumen above and the urinary space below (Haraldsson et al., 2008). Scale bars: 100 nm.

1.2 Physiological structures of the endothelial cell layer, the glomerular basement membrane and the epithelial cell layer of the glomerular capillary wall.

As aforementioned, physiological structures of different cellular layers of the glomerular capillary wall are different. The endothelial cell layer has large hour-glass-shaped fenestrated area filled glycosaminoglycan (GAG) which has negative charges (Mattern, 2008). This leads researchers to believe that the endothelial cell layer plays a crucial role in charge-selectivity of the glomerular barrier, whereas its role in size-selectivity remains questioned. The glomerular basement membrane (GBM) is a gel-like fibrous network that acts as a back-bone of the barrier. Its thickness is about 200 – 400 nm in rats and 400-600 nm in human. The epithelial cell layer consists of epithelial foot processes (commonly referred to as podocytes) with their interconnecting slit diaphragm which is a planar arrangement of fibers. The size and shape of the spacing between these interconnecting fibers remains a research topics up until today. Traditionally thought to be the most crucial layer regarding size-selectivity of the glomerular capillary wall, recent observations employing scanning electron microscopy (SEM) which reported much larger spacing between fibers, have brought about a debate about the contribution of the epithelial cell layer to solute restriction.

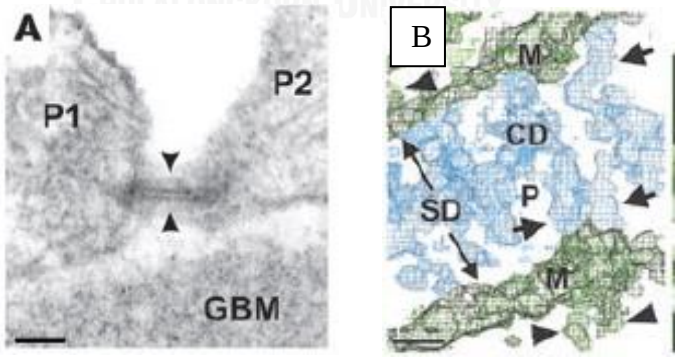

Figure 1.3 (A) Electron micrographs showing cross section of the epithelial cell layer between human podocytes (P1, P2) with the double-layered slit diaphragm (indicated by the arrows). Scale bars: 50 nm. (B) Front view of human slit diaphragm from electron tomography. Scale bars: 10 nm (Wartiovaara et al., 2004).

1.3 Contributions of cellular layers to glomerular hydraulic permeability

The total hydraulic permeability of glomerular capillary wall is the averaged fluid velocity (<*V*>) per unit pressure difference (ΔP). Their relationship can be written as following.

$$\Delta P = \frac{1}{k}\langle V \rangle \tag{1.1}$$

Likewise, the hydraulic permeability of each cellular layer is the ratio between the averaged fluid velocity through that layer and the pressure drop across that cellular layer, and the relationship between the fluid velocity and the pressure drop across the cellular layer are shown below.

$$\Delta P_{en} = (\frac{1}{k_{en}})\langle V_{en} \rangle \tag{1.2a}$$

$$\Delta P_{GBM} = (\frac{1}{k_{GBM}})\langle V_{GBM} \rangle \tag{1.2b}$$

$$\Delta P_{ep} = (\frac{1}{k_{ep}})\langle V_{ep} \rangle \tag{1.2c}$$

where ΔP_{en}, ΔP_{GBM} and ΔP_{ep} are the pressure difference across the endothelial cell layer, the GBM and the epithelial cell layer, respectively. <V_{en}>, <V_{GBM}> and <V_{ep}> are the averaged fluid velocity through the endothelial cell layer, the GBM and the epithelial cell layer, respectively. k_{GBM} is the hydraulic permeability of the glomerular basement membrane, whereas k_{ep} and k_{en} are the hydraulic permeability of the endothelial and the epithelial cell layers.

The total pressure drop across the glomerular capillary wall is the sum of ΔP_{en}, ΔP_{GBM} and ΔP_{ep}. From conservation of mass, the averaged fluid velocity, <*V*>, must equal to the averaged fluid velocity of each successive cellular layer; <V_{en}>, <V_{GBM}> and <V_{ep}>. Combining Eqs. (1.1) and (1.2a) - (1.2c), we obtain

$$\Delta P = \left(\frac{1}{k_{en}} + \frac{1}{k_{GBM}} + \frac{1}{k_{ep}} \right) \langle V \rangle \tag{1.3}$$

Therefore, the contributions to *k* from k_{en}, k_{GBM} and k_{ep} are as follows:

$$\frac{1}{k} = \frac{1}{k_{en}} + \frac{1}{k_{GBM}} + \frac{1}{k_{ep}} \tag{1.4}$$

where k_{ep}, the hydraulic permeability of the epithelial cell layer, is the product between the GBM surface fraction not covered by the podocytes (ε_s) and the averaged hydraulic permeability of the slit diaphragm, $<k_s>$.

$$k_{ep} = \varepsilon_s < k_s > \tag{1.5}$$

Analogously, k_{en}, the hydraulic permeability of the endothelial cell layer, is the product of the surface fraction of the fenestrae (ε_f) and the hydraulic permeability of the endothelial fenestrae, k_f.

$$k_{en} = \varepsilon_f k_f \tag{1.6}$$

Embedded in equation (1.5) and (1.6) is an assumption that there is no transcellular flow. Micropuncture experiments indicate that k is approximately 3-5 nm/s/Pa for rats (Deen, Lazzara, & Myers, 2001), whereas the human glomerular permeability estimated from glomerular filtration rate is a bit lower at 1.61-4.54 nm/s/Pa (Drumond & Deen, 1994). The Darcy permeability of the GBM is in the range of 1-3 nm^2, resulting in k_{GBM} being 3-9 nm/s/Pa for rats and 1.7-5.3 nm/s/Pa for normal human, indicating that the GBM is a barrier that significantly contributes to fluid transport restriction. The contributions of the endothelial and epithelial cell layer are yet unknown, and it is one of our objectives to estimate k_{en} and k_{ep} based on the structure of both layers as mentioned in Section 1.2.

1.4 Contributions of cellular layers to restriction of macromolecule transport

The experimentally measurable quantity often employed in characterizing transport of macromolecules through the glomerular barrier is the sieving coefficient, θ, the ratio between the upstream solute concentration in blood stream in the capillary

lumen (C_{blood}) and the downstream solute concentration in primary urine in Bowman's capsule (C_{urine}).

$$\theta = \frac{C_{blood}}{C_{urine}} \tag{1.7}$$

The overall glomerular sieving coefficient is simply the product of the sieving coefficient of the three layers as following.

$$\theta = \theta_{en}\theta_{GBM}\theta_{ep} \tag{1.8}$$

where θ_{en}, θ_{GBM} and θ_{ep} are the sieving coefficient of the endothelial cell layer, the GBM and the epithelial cell layer, respectively. The work presented here aims at determining the contribution of each layer to the overall glomerular sieving of rigid electrically neutral spherical solutes, and comparing the calculated result with the sieving coefficient of ficoll (highly cross-linked polysaccharide that is spherical, uncharged and not absorbed in the glomerular tubule) obtained from *in vivo* urinalnalysis.

1.5 Existing Literature

จุฬาลงกรณ์มหาวิทยาลัย
Chulalongkorn University

The contribution of each cellular layer to the size-based solute restriction of the glomerular capillary wall has been investigated for several decades, and continues to generate interest among researchers. Earlier mathematical models were done under the assumption that the glomerular barrier is a porous membrane consisting of long parallel cylindrical pores with the pore density and the effective pore radius being the pore density and pore radius which gave the correct solute sieving as reviewed by Maddox et al. (1992). Even though this model is easy to apply to the filtration data, it does not reflect the actual physiological structure of the glomerular barrier or its change due to renal disorders.

Proposed mathematical models include the heteroporous model (Deen, Bridges, Brenner, & Myers, 1985) where the membrane pores are assumed to be multi-sized, and the distributed two-pore model or the log-normal distribution +

shunt model (Öberg & Rippe, 2014) where the membrane pores are categorized into "small heterogeneous pores" of which radii follow the log-normal distribution, and "large shunt" or large pores that do not restrict solute transport. Another proposed mathematical models is the fiber matrix model(Curry & Michel, 1980) where the glomerular barrier is viewed as a fibrous medium with uniform-sized fibers. This attempt was followed by the introduction of the gel-membrane model, where the glomerular capillary wall was modeled as a charged fibrous medium and an electrically neutral porous membrane in series(Ohlson et al., 2001). The discussion about the existing mathematical simulation can be found in the book Mathematical Modeling in Renal Physiology (Layton & Edwards, 2014).

Among all the proposed mathematical models, Drumond and Deen (1995) and Edwards and Deen (1999) introduced an ultrastructural model where the glomerular capillary wall consisted of three cellular layers, resembling the physiological structure of the mammal glomerular barrier as described in Section 1.2, but the calculation was completed under an assumption that only the epithelial cell layer and the GBM contributed to the glomerular size-selectivity with the contribution of the endothelial cell layer negligible because the size of the fenestrae is much larger than the protein radii. In the work presented here, the ultrastructural model as pioneered by Edwards and Deen (1999) is employed, but with an assumption that the endothelial cell layer also plays a significant role in glomerular size-selectivity as evidenced by more recent experimental results (Jeansson & Haraldsson, 2003).

1.6 Model formulation

1.6.1 Ultrastructural model (modified to include an endothelial cell layer)

A traditional view of glomerular size-selectivity is that the crucial role is played by the epithelial slit, whereas the contributions of the GBM and the endothelial cell layer are still debated. In this work, all three cellular layers are taken into account. The endothelial cell layer is modeled as full of fenestrae filled with glycoaminoglycan

(GAG) as shown schematically in Fig. (1.4), whereas the second layer, GBM, is viewed as a fibrous medium containing multiple-sized fibers. The epithelial slit diaphragm is assumed to be a row of parallel cylinders with sizes of spacing between adjacent fibers follows the distribution function reported from recent observation from scanning electron microscopy (Gagliardini et al., 2010; Rice et al., 2013). The calculated solute sieving will be compared to the sieving of ficoll solutes through an isolated GBM(Bolton, Deen, & Daniels, 1998) as well as the total sieving of ficoll solutes through human glomerular barriers obtained from *in vivo* urinalnalysis (Blouch et al., 1997).

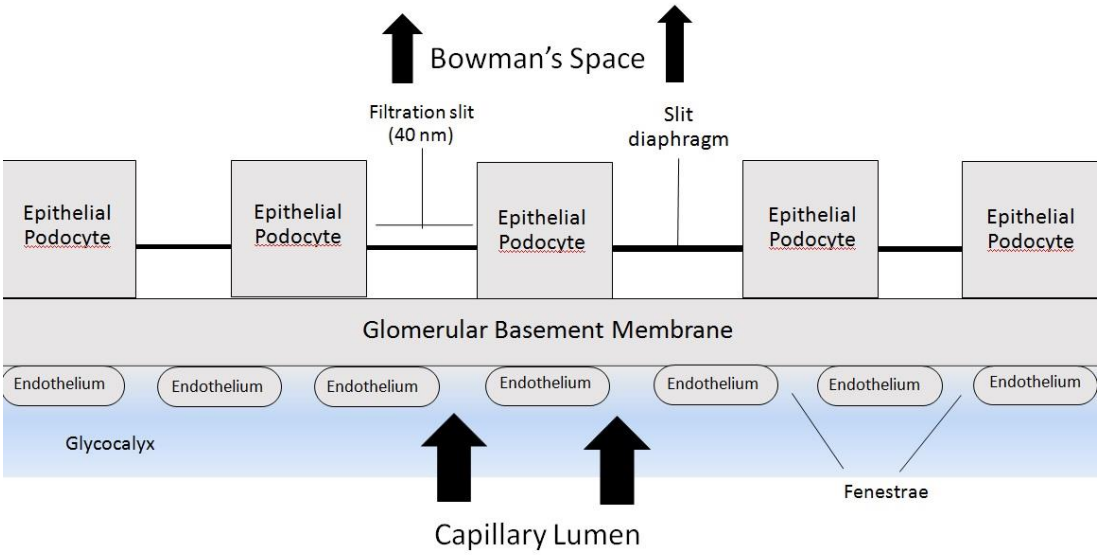

Figure 1.4 Schematic drawing of an ultrastructural model of the glomerular capillary wall introduced by Drumond, Deen and Edwards(Drumond & Deen, 1995; Edwards, Daniels, & Deen, 1997). The glomerular barrier consists of the endothelium cell layer, glomerular basement membrane (GBM) and the epithelial cell layer with the slit diaphragm connecting the podocytes. The arrows indicate the direction of fluid flow. Figure is not drawn to scale.

1.6.2 Thesis and methodology overview

Chapter 2 is dedicated to a calculation of solute filtration through an epithelial slit modeled as a row of parallel rigid cylinders with non-uniform spacing between adjacent fibers. The dimensionless flow resistance (ΔP_{ep} scaled with viscous stress) is calculated using a commercial finite element method (COMSOL Multiphysics, Stockholm, Sweden) to solve the Stokes and continuity equations. The distribution function of gaps between fibers is assumed to follow the log-normal distribution with the average and the standard deviation of the gap-width being values reported from electron microscopy. The sieving coefficient through the epithelial cell layer (θ_{ep}) is obtained as the averaged sieving coefficient through the slit diaphragm ($<\theta_{SD}>$), and, to examine the controversy arisen from electron microscopy observations regarding to the size of spacing between fibers, the implication of the difference in the sizes of the gap-width between fibers of the slit diaphragm is investigated.

In Chapter 3, the calculation of solute transport in the glomerular basement membrane is given in details. Similarly to the work of Drumond and Deen (1995) and Edwards and Deen (1999), the GBM is modeled as an isotropic medium with the solute concentration and the sieving coefficient (θ_{GBM}) obtained by solving a one-dimensional convection-diffusion equation analytically(Drumond & Deen, 1995; Edwards, Daniels, & Deen, 1999). The difference between previous studies employing an ultrastructural model and our work regarding solute transport in the GBM is that they employed an empirical formular for the reduced solute diffusivity and the changed convective rate, whereas we obtained expressions for these hindrance factors by investigating the effect of the hydrodynamic interaction between solutes and fibers in the GBM. The reduced diffusivity and sieving coefficient through the GBM is presented as a function of solute radii and compared with ficoll sieving from ultrafiltration through an isolated GBM.

The effect of an endothelial cell layer, the cellular layer previously not included in an ultrastructural model, is examined in Chapter 4. Similarly to filtration through the GBM, the sieving coefficient through the endothelial cell layer (θ_{en}) is determined by solving the one-dimensional convection-diffusion equation analytically, with the

calculation of the hindrance factors being similar to those of the GBM. Due to lack of information regarding the concentration of fibers (glycoaminoglycan or GAG) within the endothelial fenestrae, the effect of the variation of the GAG volume fraction on θ_{en} is examined.

After obtaining the sieving coefficient of the three cellular layers, the total sieving coefficient is calculated and compared to sieving coefficients of ficolls obtained experimentally from *in vivo* urinanalysis in human; these details are given in Chapter 5. In addition to obtaining the correct sieving coefficient, the assumptions employed in its calculation should also yield a correct hydraulic permeability that falls within the range of values estimated from glomerular filtration rate. The contribution of each cellular layer to glomerular fluid filtration will be discussed extensively in Chapter 6. The effect of the absence of each cellular layer on glomerular size-selectivity, as well as its medical implication, would be discussed in Chapter 7. Finally, the thesis summary and conclusion will be presented in Chapter 8.

จุฬาลงกรณ์มหาวิทยาลัย
Chulalongkorn University

Chapter 2
Transport of Macromolecules through the Glomerular Epithelial Slit

The observation employing transmission electron microscopy of the epithelial slit(Rodewald & Karnovsky, 1974) led many researchers to believe that the epithelial slit was the most restrictive barrier for solute transport due to its averaged gap-width between fibers being almost two-times smaller than radii of biomarkers such as albumin. However, more recent electron microscopy observations with wider gap-width between fibers seen in the slit diaphragm (Gagliardini et al., 2010; Rice et al., 2013) gave rise to a controversy about the contribution of epithelium to solute restriction. In this chapter, solute filtration through the slit diaphragm is investigated through mathematical simulation employing distribution functions of fiber spacing based on electron microscopy observation from different techniques. In Section 2.1, the dimensions and structure of the epithelial slit observed from electron microscopy are extensively discussed. The mathematical formulation is presented in Section 2.2; the modified Stokes-Einstein equation and the convection-diffusion equation for spheres transported through a row of parallel cylinders with uniform spacing is discussed in Section 2.2.1, whereas the averaging process of the sieving coefficient through a row of parallel fibers with non-uniformed spacing is presented in Section 2.2.2. The calculation of the dimensionless flow resistance using finite element method is discussed in details in Section 2.2.3, and the numerical procedure and parameters employed in our simulation are given in Section 2.2.4. The averaged sieving coefficient through the slit diaphragm with the fiber spacing following these distributions is presented as a function of solute sizes in Section 2.3.

2.1 Structure of the epithelial slit

The distribution function and sizes of spacing between fibers in the epithelial slit has been a debate topic for several decades due to differences in obtained

micrographs. The earliest image of the epithelial slit structure was reported by Rodewald and Karnovsky (1974) using transmission electron microscope (TEM) as a "zipper" configuration with a central filament and alternative cross-bridges on either sides. From the obtained micrograph, they estimated the sizes of the "gap" between fibers to be 4x14 nm.

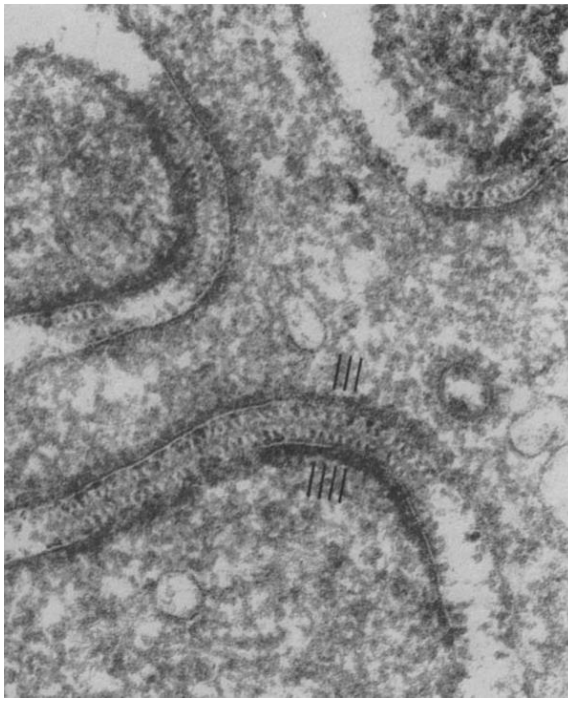

Figure 2.1 Image of slit diaphragm (indicated by arrows) from transmission electron microscopy (Rodewald & Karnovsky, 1974).

Their observation was supported by the work of Wartiovaara et al. (2004) where the slit structures of Sprague-Drawley rats as well as those of healthy humans and patients with nephrotic syndrome of the Finnish type were reconstructed using electron tomography, and found to be the zipper configuration in an approximate sense with dimensions similar to those reported by Rodewald and Karnovsky (1974).

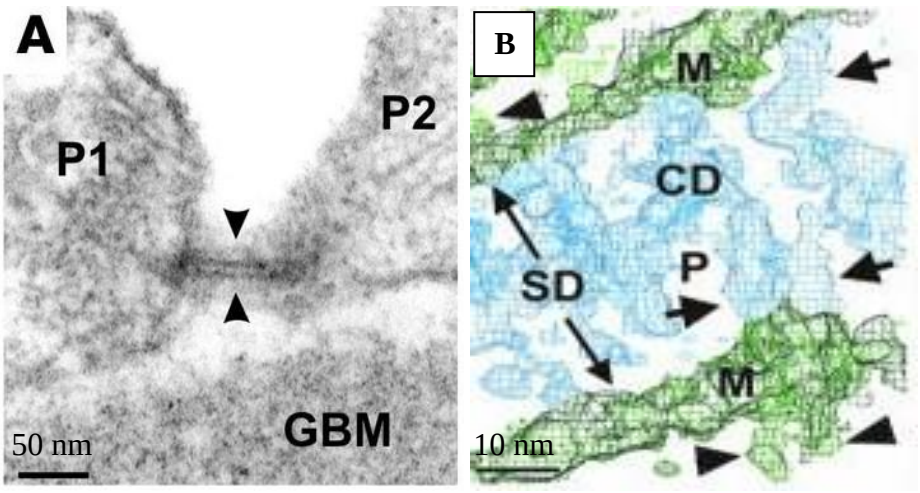

Figure 2.2 images of slit diaphragm from electron tomography(Wartiovaara et al., 2004) (A) side view (B) top view

Apart from the zipper configuration, another configuration called the "ladder" configuration was proposed by Hora et al. (1990) where the interconnecting fibers were found to span the entire distance between podocytes without the central filament. An observation twenty years later using scanning electron microscopy (SEM) by Gagliardini et al. (2010) found that the central filament was not presented in the slit diaphragm, but the gaps between these fibers are more of elongated pores as shown below in Fig. (2.3). After examining 600 pores, they conclude that the pore radii follow the log-normal distribution as shown in Fig. (2.4A) and (2.4B). The mean radii reported (12.10 nm for Wistar rats and 11.42 nm for Munich-Wistar Fromter rats) is 6 times larger than dimensions reported earlier by Rodewald and Karnovsky (1974) and Wartiovaara et al. (2004).

The most recent observation was completed by Rice et al. (2013) where the images of the structure of the epithelial slit diaphragm of Sprague Dawley is obtained at higher resolution from helium ion scanning microscopy as shown below in Fig. (2.5), where the slit diaphragm structure seems to be the "ladder" configuration but with u reported as 22.0 ± 8.0 nm.

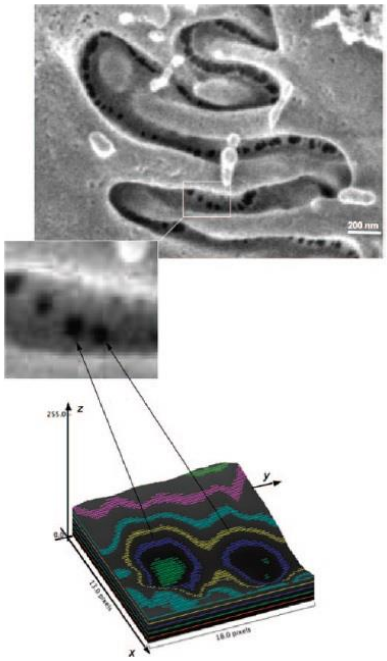

Figure 2.3: Slit diaphragm structure of the glomerular capillary wall obtained by SEM(Gagliardini et al., 2010).

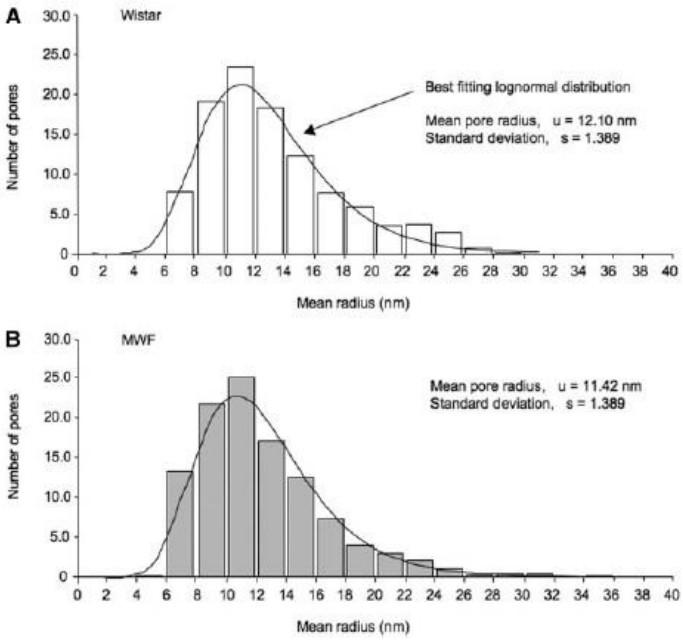

Figure 2.4: Distribution of pore radii of the epithelial slit diaphragms of (A) Wistar rats and (B) Munich-Wistar Fromter rats from SEM(Gagliardini et al., 2010).

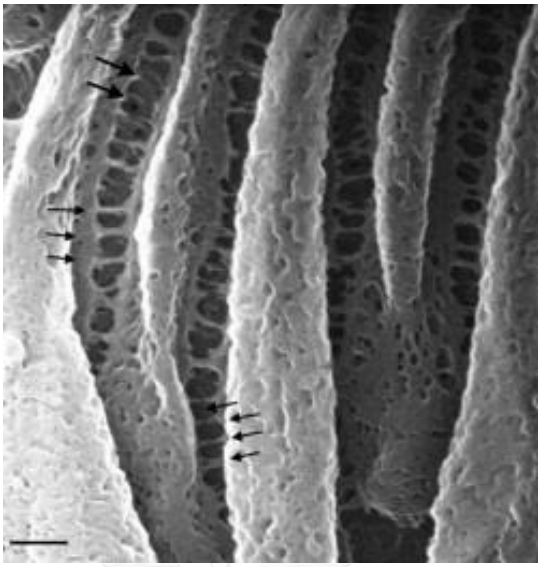

Figure 2.5: Structure of the epithelial slit diaphragm obtained from helium ion microscopy(Rice et al., 2013) Scale bar: 100 nm

Rice et al. (2013) attributed the possible explanation for the difference between the gap sizes they reported and those of Gagliardini et al. (2010) to be the different dehydration technique. However, to ascertain the quality of the magnification of the helium ion microscopy, they also imaged the slit diaphragm using SEM, and found the structure to be less defined.

As discussed above, electron microscopy observations (Gagliardini et al., 2010; Rice et al., 2013; Rodewald & Karnovsky, 1974; Wartiovaara et al., 2004), there were two possible configurations for structure of interconnecting tissue layer between two podocytes in epithelial cell layer: the zipper and the ladder configurations. In our simulation, we modeled the slit diaphragm based on the "ladder" configuration by assuming that it is a row of parallel fibers albeit with non-uniform spacing. The gap-width between adjacent fibers are assumed to follow a log-normal distribution with parameters based on observations from electron microscopy. The mathematical model will be discussed further in the next section.

2.2 Mathematical model

As mentioned earlier, the outer most layer, the epithelial cell layer, consists of podocytes interconnected by planar arrangement of fibers called the slit diaphragm. Assuming that there is no transcellular solute transport, the sieving coefficient of the epithelial cell layer is simply the sieving coefficient through the slit diaphragm. Based on the observation of Hora and colleagues(Hora, Ohno, Oguchi, Furukawa, & Furuta, 1990)and more recent results from helium ion microscopy of Rice et al. (2013), the slit diaphragm is modeled as a row of parallel cylinders with the important geometric parameters as shown in Fig. (2.6).

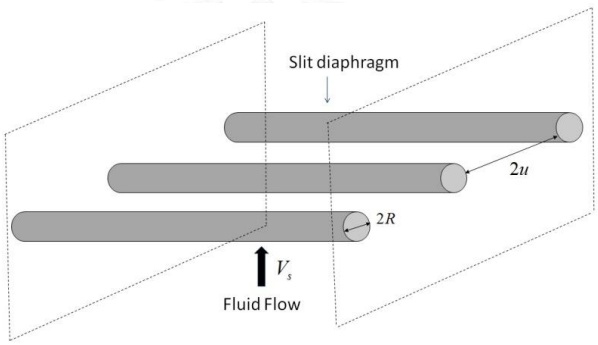

Figure 2.6: The slit diaphragm modeled as a row of parallel cylindrical fibers. V_s is the fluid velocity through the slit diaphragm, and R is the fiber radius. u is the half-width of the spacing between adjacent fibers. L, the distance between centerlines of fibers, = $u + R$.

2.2.1 Sieving through a row of parallel cylinders with uniform spacing

Sieving coefficient through the epithelial slit (θ_{ep}) is the ratio between the solute concentration in urine in Bowman's space(C_{urine}) to that between the GBM and the epithelium (C_{GBM-ep}) . It can be written as follows:

$$\theta_{ep} = \frac{C_{urine}}{C_{GBM-ep}} \tag{2.1}$$

θ_{ep} can be calculated by determining the solute concentration through a row of parallel cylinders. The solute concentration at any point is determined by the balance between chemical potential gradient and hydrodynamic force shown below.

$$-kT\nabla \ln C - 6\pi\eta r_s(\mathbf{f}\cdot\vec{U} - \mathbf{g}\cdot\vec{V}) = 0 \tag{2.2}$$

where k is Boltzmann constant. T is absolute temperature, whereas $\vec{U}$ is solute velocity, and $\vec{V}$ is the fluid velocity. r_s is the solute radius, and η is the fluid viscosity. **f** and **g** are second-order tensors which contain force coefficients. f_{ij} is the force in the i-th direction on a sphere moving in the j-th direction, whereas g_{ij} is the force in the i-th direction on a stationary sphere due to fluid motion in the *j-th* direction. In absence of the hindering row of cylinders, **f** and **g** are simply the identity tensors, and Eq. (2.2) is the Stokes-Einstein equation. Based on the above equation, the solute flux is

$$\vec{N} = C\vec{U} = -\mathbf{f}^{-1}\cdot\left[D_\infty\vec{\nabla}C - \mathbf{g}\cdot\vec{V}C\right] \tag{2.3}$$

where D_∞ , the solute diffusivity, is the ratio between the thermal energy (kT) and the Stokes' drag coefficient ($6\pi\eta r$). The pseudo-steady convection-diffusion equation can be written as

$$\vec{\nabla}\cdot\vec{N} = \frac{\partial C}{\partial t} \approx 0 \tag{2.4}$$

Drumond and Deen (1995) solved the steady-state convection equation for spheres moving through a row of parallel fibers with uniform spacing. Their expression for the sieving coefficient, to good approximation, is as follows.

$$\theta_{SD} = \frac{1-\lambda}{1-\left[1-\exp(-Pe_{Slit}L_{GBM-Slit}/R)\left(1-\exp(-APe_{Slit})\right)\lambda\right]} \tag{2.5}$$

where $\lambda = r_s/u$. Other parameters appeared in Eq. (2.3) are defined as

$$Pe = \frac{VR}{D_\infty} \tag{2.6}$$

where V is the magnitude of the undisturbed fluid velocity far from the hindering row of parallel cylinders.

$$A = \frac{3.65}{R/L} + \frac{0.573}{u/L} \tag{2.7}$$

Drumond and Deen (1995) also demonstrated that the sieving coefficient through a row of parallel cylinders with uniform spacing with its sharp cut-off cannot explain the more slowly declining profile of the sieving coefficient obtained as a function of solute sizes from *in vivo* urinalysis. This indicated that the spacing between adjacent fibers of the slit diaphragm was likely to be non-uniform. The next section is dedicated to the averaging procedure of the sieving coefficient through these non-uniform gaps.

2.2.2 Averaged sieving coefficient through a row of parallel cylinders with non-uniform spacing

Following the formulation of Drumond and Deen (1995), if the non-uniform spacing between adjacent fibers of the slit diaphragm follows the distribution function $g(u)$, the sieving coefficient of the slit diaphragm can be written as

$$\theta_{ep} = \langle \theta_{SD} \rangle = \int_0^\infty \theta_{SD}(u) G(u) du \tag{2.8}$$

where $G(u)$ is the product between $g(u)$ and the weighting factor, $q(u)$, defined as

$$q(u) = \frac{(u+R)^2}{f_T} \tag{2.9}$$

where the dimensionless flow resistance, f_T, is the ratio between the pressure difference and the viscous stress within the fluid:

$$f_T = \frac{\Delta P_S}{\eta V_s / L} \tag{2.10}$$

q (u), therefore, is $=\eta V_s\left(u+R\right)/\Delta P_s$. It accounted for the dependence of the flow rate on the gap half-width, u, for a given pressure difference. Given that $\int_0^\infty G(u)du=1$, the averaged sieving coefficient is

$$\theta_{ep}=\left\langle\theta_{SD}\right\rangle=\frac{\int_0^\infty\left(u+R\right)^2\theta_{SD}(u)\,f_T^{-1}g(u)du}{\int_0^\infty\left(u+R\right)^2\,f_T^{-1}g(u)du} \tag{2.11}$$

θ_{SD} is given as a function of u in Eq. (2.5) - (2.7). The calculation of the dimensionless flow resistance is done by solving the Stokes equation as explained in the next section. Once the distribution function, *g (u)*, is known, $\left\langle\theta_{SD}\right\rangle$ can be calculated.

2.2.3 Calculation of dimensionless flow resistance

In this work, the slit diaphragm is modeled as a row of parallel cylinders with non-uniform spacing attached to a pair of parallel plates. The Reynolds number characterizing the filtration process through the glomerular capillary wall is known to be very low. Viscous dissipation dominates the system. We employed the formulation introduced by Drumond and Deen (1995) where the dimensionless flow resistance, f_T, of the epithelial slit is

$$f_T = f + f_P . \tag{2.12}$$

where f_P is the dimensionless flow resistance of a Poiseuille flow between parallel plates written as following:

$$f_P=\frac{3L_{GBM-Slit}L}{W_P{}^2} \tag{2.13}$$

where L, the distance between the centerlines of two adjacent cylinders, is $u+R$. W_p is the half distance between two podocytes, and $L_{GBM\text{-}Slit}$ is the distance between the GBM and slit diaphragm.

f is the dimensionless flow resistance of a flow past a row of parallel cylinders. In other words, the slit diaphragm is modeled as a row of parallel cylinders connecting two parallel walls (with the parallel walls being the simplification of the podocyte surfaces). Because the Reynolds number characterizing the flow through the epithelial slit is small, the relationship between fluid velocity, V_s , and pressure drop, $(\Delta P)_s$, in Eq. (2.10) can be obtained by solving the Stokes and continuity equations for a flow past a row of parallel cylinders by using the commercial finite element package (COMSOL Multiphysics, Stockholm, Sweden). The calculated pressure at any point was shown in Fig. 2.7.

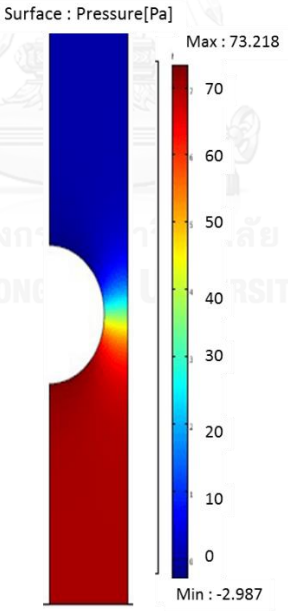

Figure 2.7 Calculated pressure from finite element solutions of Stokes and continuity equation.

From the difference between upstream and downstream pressure, the dimensionless flow resistance was determined from the dimensionless form of Eq. (2.10) as following:

$$f = (\hat{u}+1)\left[\hat{P}_{upstream} - \hat{P}_{downstream}\right] \tag{2.14}$$

where $\hat{P}$ is the dimensionless pressure $\left(\hat{P} = P/\left[\eta V_{upstream}/L\right]\right)$ and $\hat{u}$ is u/R.

The dimensionless flow resistance, f, is shown as a function of $u/u+R$ below in Fig. (2.8). Our results agree very well with previous calculations (Drumond & Deen, 1994), and the lubrication approximation(Sangani & Acrivos, 1982), confirming the accuracy of the finite element solution. Because results from previous calculation are only available for $0.1 \le 1-\frac{R}{L} \le 0.9$, we extended our calculation to include the range of $1-\frac{R}{L}$ from 0.9 to 1.

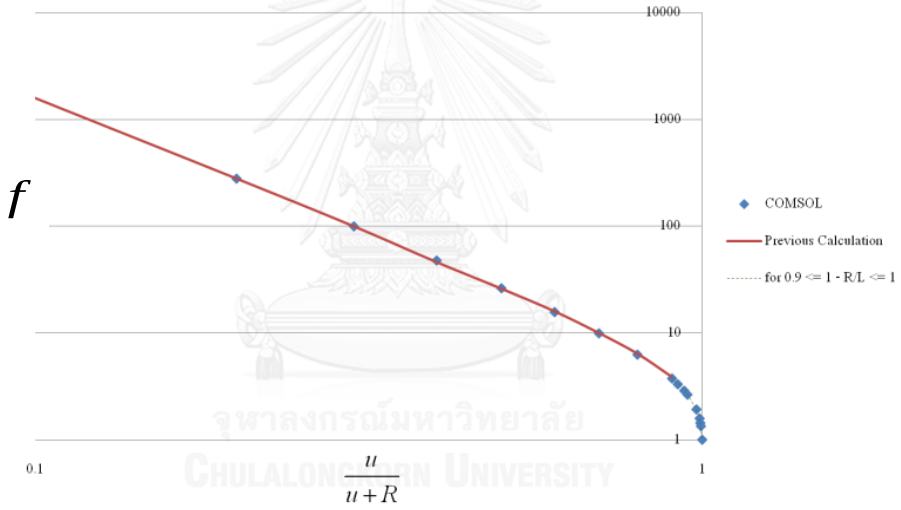

Figure 2.8: f calculated from finite element solutions of the Stokes and continuity euqations (blue dots) are compared to previous calculation of Drumond and Deen (1994) indicated as a red line.

For convenience, expressions for f as a function of R/L has been obtained. When the gap between fibers is small, Drumond and Deen (1994) found that f was well approximated by

$$f = A(1-\frac{R}{L})^{B} \tag{2.15}$$

where $A = \frac{9\pi}{4\sqrt{2}}$ and $B = -2.5$. This expressions is accurate to within 3 percent for $0.7 \le \frac{R}{L} \le 1$. For less closely spaced fibers, the dimensionless flow resistance is, to a good approximation,

$$f = 10^{C} \tag{2.16}$$

where $C = 0.336 + 2.74(\frac{R}{L}) - 2.74(\frac{R}{L})^2 + 3.16(\frac{R}{L})^3$ which is accurate to within 4 % for $0.1 \le \frac{R}{L} \le 0.7$.

Equations (2.14) and (2.15) have not covered all ranges of *R*/*L* needed with the range of $\frac{R}{L}$ from 0 to 0.1 missing. Therefore, we used nonlinear regression (MATLAB v. R2001b software, Mathwork, Netick, MA, USA) to obtain the following expressions from *f* we obtained from finite element solution:

$$f = D(1 - \frac{R}{L})^{E} + F \tag{2.17}$$

where $D = -7.729, E = 3.463$ and $F = 9.133$. This expression is accurate for $0.02 \le \frac{R}{L} \le 0.1$. For less closely spaced fibers, the dimensionless flow resistance can be written as

$$f = G(1 - \frac{R}{L})^{H} + I \tag{2.18}$$

where $G = -1.246, H = 81.05$ and $I = 2.16$ which is valid for $0 \le \frac{R}{L} \le 0.02$.

Chulalongkorn University

2.2.4 Numerical procedure and employed parameters

In this work, *g* (*u*) is assumed to follow the log-normal distribution:

$$g(u) = \frac{1}{u\sigma\sqrt{2\pi}} e^{-\frac{(\ln u - \mu)^2}{2\sigma^2}} \tag{2.19}$$

where μ and σ are constants. Three different sets of parameters would be employed as following:

(1) the mean value of u, $<u>$, = 12.10 nm and its standard deviation, $\sqrt{<u^2>}$, = 1.389 nm as reported by Gagliardini et al. (2013). $g(u)$ as a function of u is shown in Fig. (2.4a)

(2) $<u>$ = 22 nm and $\sqrt{<u^2>}$ = 4 nm as reported by Rice et al. (2013). $g(u)$ as a function of u is shown below in Fig. (2.9).

(3) $<u>$ = 2 nm as reported by Rodewald and Karnovsky (1974) and Wartiovaara et al. (2004) with $\sqrt{<u^2>}$ varied from 0.7 to 4 nm (Fig. 2.10).

After the expressions for f_T, $g(u)$ and θ_{SD} have been determined, we obtained the averaged sieving coefficient through the slit diaphragm ($<\theta_{SD}>$) by integrating the integrand specified in Eq. (2.11) using recursive adaptive Simpson quadrature command known as the quad command (MATLAB v. R2001b software, Mathwork, Netick, MA, USA). Based on electron-microscopy observation, the fiber radii, R, is set at 6.5 nm. W_p is set at 21 nm, and $L_{GBM\text{-}Slit}$ is assumed to equals 70 nm.

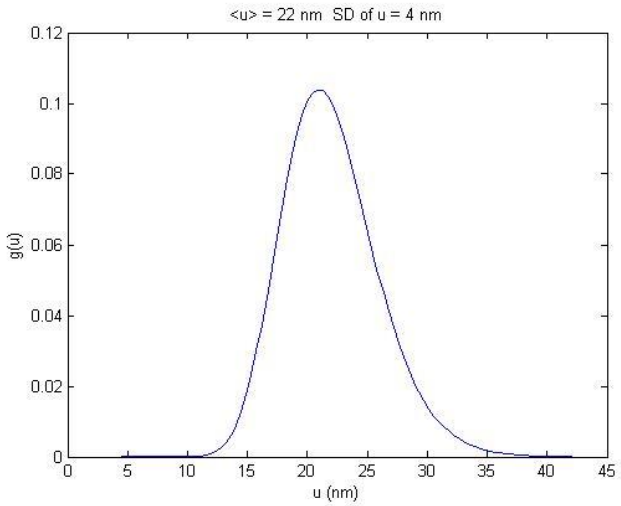

Figure 2.9 Log normal distribution, g (u), as a function of u. $<u>$ = 22 nm and $\sqrt{\langle u^2 \rangle}$ = 4 nm.

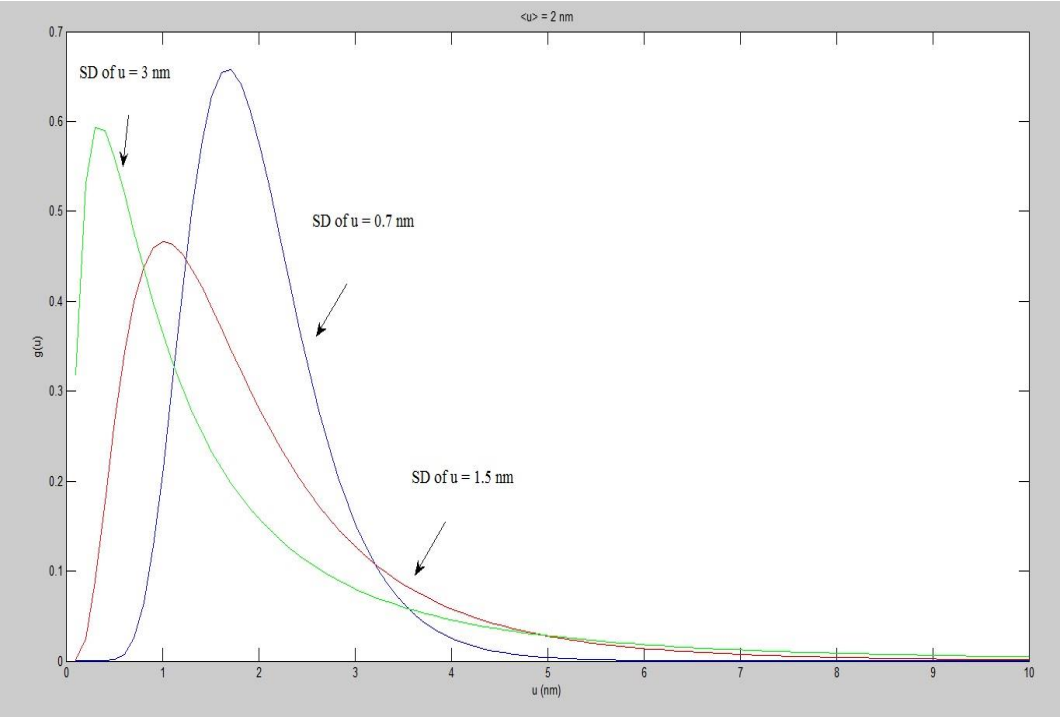

Figure 2.10 Log normal distribution, $g(u)$, as a function of u. $\langle u \rangle$ = 2 nm and $\sqrt{\langle u^2 \rangle}$ = 0.7, 1.5 and 3 nm, respectively.

จุฬาลงกรณ์มหาวิทยาลัย
Chulalongkorn University

2.3 Results: calculated sieving coefficient through the slit diaphragm

Shown below in Fig. (2.11) are $\langle \theta_{SD} \rangle$ as functions of sphere radii calculated by assuming that $\langle u \rangle$ = 12.10 nm (solid line) and $\langle u \rangle$ = 22 nm (dashed line), respectively. As expected, $\langle \theta_{SD} \rangle$ are very close to 1 for both values of mean fiber half-spacing, with $\langle \theta_{SD} \rangle$ calculated by assuming that $\langle u \rangle$ = 22 nm being slightly larger. This is due to the fact that both values of $\langle u \rangle$ are more than twice as large as the maximum solute radii (5.6 nm) shown in the figure. This indicates that, if $\langle u \rangle$ is 12.10 nm or larger as reported from SEM and helium ion microscopy, the slit diaphragm almost does not contribute to solute restriction.

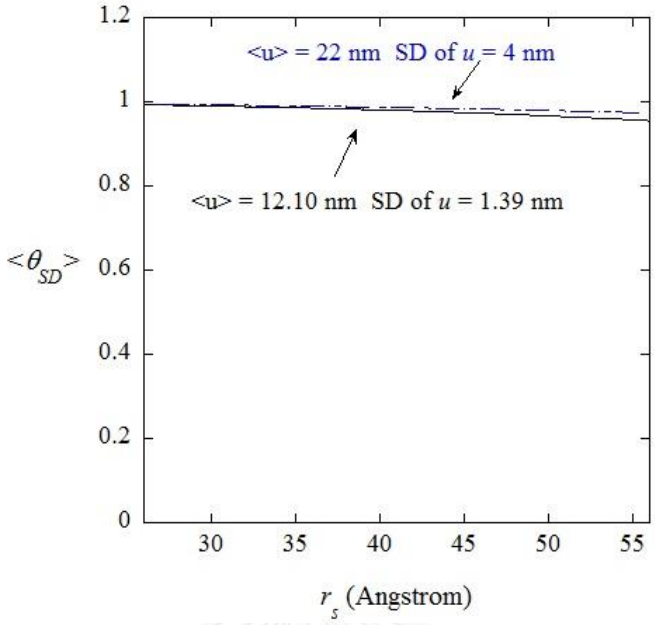

Figure 2.11 Calculated sieving coefficients through slit diaphragm as functions of solute radii. Results are plotted for <*u*> = 12 nm (solid line). <*u*> = 22 nm (dashed line).

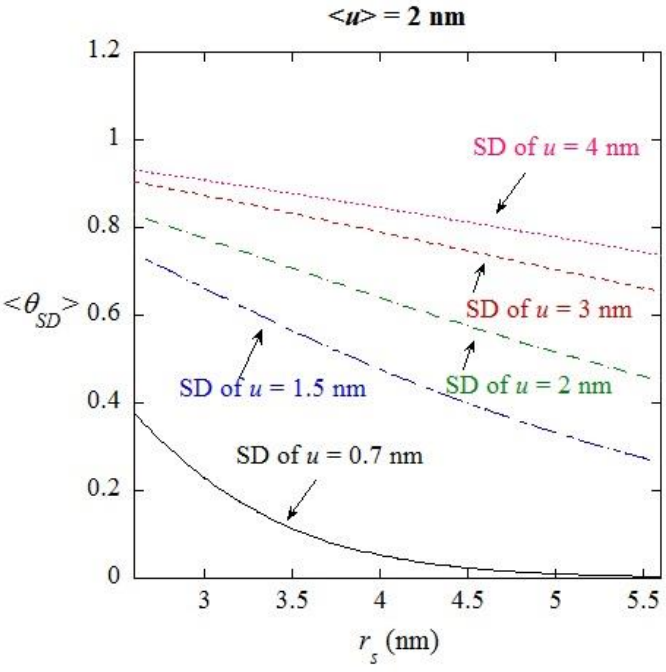

Figure 2.12 Calculated sieving coefficients through slit diaphragm as functions of solute radii. Results are plotted for <*u*> = 2 nm and $\sqrt{\langle u^2 \rangle}$ = 0.7, 1.5, 2, 3 and 4 nm.

If the mean value of the half-spacing between cylinders is reduced to 2 nm as reported by Rodewald and Karnovsky (1974) and Wartiovaara et al. (2004), we found that the value of $<\theta_{SD}>$ strongly depends on the standard deviation of u. If $\sqrt{\langle u^2 \rangle}$ = 0.7 nm, $<\theta_{SD}>$ is quite small, indicating that the slit diaphragm is restrictive to solute transport. For instance, $<\theta_{SD}> = 0.096$ for $r_s = 3.6$ nm (the radii of albumins). However, as $\sqrt{\langle u^2 \rangle}$ increases, so does $<\theta_{SD}>$. If $\sqrt{\langle u^2 \rangle}$ is as large as 4 nm, $<\theta_{SD}>$ can be as high as 0.87 for solute with $r_s = 3.6$ nm. This contradicts the previously held belief that the slit diaphragm is the most restrictive layer due to the fact that $<u>$ = 2 nm. In short, it is possible for more than 80% of spherical particles with sizes comparable to proteins such as albumin to be filtered through the slit diaphragm if $\sqrt{\langle u^2 \rangle}$ is high enough. To verify the role that the slit diaphragm plays in glomerular size-selectivity, the next step is to use the obtained $<\theta_{SD}>$ to calculate the sieving coefficients through the GBM and the endothelial cell layer to determine the overall glomerular sieving coefficient and compare it with sieving of ficoll from urinalysis performed in healthy human.

จุฬาลงกรณ์มหาวิทยาลัย
Chulalongkorn University

Chapter 3
Transport of Macromolecules through Glomerular Basement Membrane

The glomerular basement membrane (GBM) is a hydrogel containing fibrous networks with thickness about 200 – 400 nm. It is the thickest layer of glomerular capillary wall, often viewed as the backbone of the glomerular barrier. The GBM is approximately 90% water by volume. Its structural integrity is maintained by a network of type IV collagen. Other presented fibers also include laminin, entactin, fibronectin and heparan sulfate proteoglycan which consists of a core protein and chains of glycoaminoglycan (GAG). According to Darcy's law, the fluid flux, q, is simply defined as

$$q = \frac{-\kappa_{GBM}}{\eta}\vec{\nabla}P \tag{3.1}$$

where κ_{GBM} is the GBM Darcy permeablity. η is the fluid viscosity and P is the fluid pressure. Deen et al. (2001) claimed that a 1:1 mixture of a "coarse" fibers or type IV collagen (of which radii are 3.5 nm) and a "fine" fibers or GAG (of which radii are 0.5 nm: too small to observe in the electron micrograph) yields the correct values of κ_{GBM} and fiber volume fraction in the GBM. It is believed that this layer play a crucial role on glomerular fluid restriction, but how the GBM affects solute filtration is still questioned.

Previously, in the ultrastructural model of Edwards and Deen (1999), the GBM was viewed as an isotropic medium with reduced diffusivity and changed convection rate obtained from empirical formula from experiment. In this thesis, the diffusive and convective hindrance factors are determined from solute-fiber hydrodynamic interaction based on existing transport theory. A pseudo-steady one dimensional convection-diffusion equation explaining solute filtration through an isolated GBM is introduced in Sect. 3.1, whereas the effect of type IV collagen and GAG on the solute diffusivity reduction is investigated in Sect. 3.2. The change in solute convection rate

within the GBM, calculated from the drag force on a freely-suspending sphere in Brinkman's medium, is discussed in Sect. 3.3, whereas the effect of cellular blockage on solute filtration through an intact GBM (a GBM still attached to the endothelial and the epithelial cell layers) is presented in Sect. 3.4. The sieving coefficients through the isolated and the intact GBM are presented as a function of solute radii in Sect. 3.5.

3.1 Isolated GBM

In the work presented here, the GBM is viewed as an isotropic fibrous medium, where the concentration of the solutes transported through the isolated GBM can be found from the pseudo-steady convection-diffusion equation:

$$\vec{\nabla}\cdot\vec{N} = \vec{\nabla}\cdot\left(-K_d D_\infty \vec{\nabla}C + K_c \vec{v}_{GBM} C\right) = 0 \tag{3.2}$$

where C is the local concentration of uncharged macromolecules. $\vec{N}$ is the solute flux, whereas D_∞ is the diffusivity of the unconfined macromolecule. $\vec{v}$ is the local fluid velocity. K_d and K_c are the diffusive and convective hindrance factors, respectively. Under the isotropy assumption, the macromolecule flux through an isolated GBM is one-dimensional, and C can be found analytically by integrating Eq. (3.2) twice with the following boundary conditions:

$$C\left(z=0\right) = \Phi C_{upstream} \ . \tag{3.3a}$$

$$C\left(z=L_{GBM}\right) = \Phi C_{downstream} \tag{3.3b}$$

where L_{GBM} is the GBM thickness. $C_{upstream}$ and $C_{downstream}$ are the bulk external upstream and downstream solute concentrations, respectively. Φ is the equilibrium partition coefficient, the ratio between the external solute concentration and the solute concentration in the GBM at $z = 0$ (upstream) and $z = L_{GBM}$ (downstream). The obtained solution results in the sieving coefficient through the GBM, θ_{GBM}, being

$$\theta_{GBM} = \frac{C(z=L_{GBM})}{C(z=0)} = \frac{\Phi K_c}{\left(1-\exp(-Pe)\right)+\Phi K_c \exp(-Pe)} \tag{3.4a}$$

where

$$Pe = \frac{\Phi K_c v_{GBM} L_{GBM}}{\Phi K_d} \quad . \tag{3.4b}$$

In order to determine θ_{GBM}, the diffusive and convective permeabilities, ΦK_d and ΦK_c, must be determined. After ΦK_d and ΦK_c are known, θ_{GBM} can be calculated directly from Eqs. (3.4a) and (3.4b).

3.2 Hindered diffusion in the GBM (ΦK_d)

Due to an absence of a calculation of a sphere diffusivity in a hydrogel consisting of two fibers of different sizes, in this work, the contributions of type IV collagen and GAG to hindered diffusion of macromolecules in the GBM is investigated based on existing theory regarding diffusion in fibrous media. Brady has proposed that the particle diffusivity in a gel-like material can be written as a product of *F*, the factor due to hydrodynamic effect, and *S*, the factor due to particle-fiber steric interaction, as following(Brady, 1994):

$$K_d = \frac{D_{GBM}}{D_\infty} = FS \tag{3.5}$$

For the hydrodynamic effect, *F*, Clague and Phillips numerically calculated the drag on a sphere confined in a random array of cylinders(Clague & Phillips, 1996). The expression from their calculation which is employed in our work was obtained from an ensemble average over many fiber configurations(Phillips, 2000) as following;

$$F(r_s, r_f, \phi) = \exp(-a\phi^b) \tag{3.6a}$$

where

$$a = 3.727 - 2.460\left(r_f / r_s\right) + 0.822\left(r_f / r_s\right)^2 \quad . \tag{3.6b}$$

$$b = 0.358 + 0.366\left(r_f / r_s\right) - 0.0939\left(r_f / r_s\right)^2 . \qquad (3.6c)$$

r_s and r_f is the sphere and fiber radius, respectively, whereas ϕ is the fiber volume fraction.

The steric factor, *S*, in Eq. (3.5) is due to the fact that the distance between the fiber surfaces and the spheres must always be larger or equal to the sphere radius. For a rigid sphere (with radius r_s) diffusing in a fibrous medium containing rigid uniform-sized fibers, Johnson et al. (1996) found that their steric interaction causes *S* to be

$$S = \exp\left(-0.84\left[\left(1 + \frac{r_s}{r_f} \right)^2 \phi \right]^{1.09} \right) \qquad (3.7)$$

The expression in Eq. (3.7) is for a steric interaction between rigid spheres and rigid cylindrical fibers. Another alternative is to set $S = 1$ due to GAG flexibility. The choice of setting $S = 1$ is supported by the fact that setting $S = 1$ had yielded correct diffusivities for spheres suspended in a dextrin solution. (Dextran is a flexible polymer.) In our work, *S* is set at 1.

The available data regarding macromolecule diffusion in the GBM is not K_d, but was obtained in the form of ΦK_d, the diffusive permeability. In our work, the partition coefficient, Φ, is calculated using the Ogston equation for dilute solution in fibrous media containing two different-sized fibers:

$$\Phi = \exp\left[-\phi_{collagen}\left(1 + \frac{r_s}{r_f^{collegen}} \right)^2 - \phi_{GAG}\left(1 + \frac{r_s}{r_f^{GAG}} \right)^2 \right] \qquad (3.8)$$

where type IV collagen radii, $r_f^{collagen}$, are 3.5 nm, and GAG radii, r_f^{GAG}, are 0.5 nm. $\phi_{collagen} = \phi_{GAG} = 0.05$. The comparison between our calculated ΦK_d and ΦK_d obtained from experiment is given below.

3.3 Hindered convection through the GBM

Due to an absence of the calculation of convective hindrance factor (K_c) of spheres suspended in a random array of fibers, in this work, K_c within the GBM is calculated from its Darcy permeability by assuming that the force on a sphere freely suspended in the GBM is that of a sphere freely suspended in the Brinkman's medium with the Darcy permeability equals to the Darcy permeability of the GBM, κ_{GBM}. The Brinkman medium approach is normally employed in calculation of fluid velocity and transport properties within porous or fibrous media, where the nanostructure of the media is either unknown or not well defined. The governing equation for fluid velocity and pressure inside such medium, often referred to as the Brinkman equation, is as following:

$$-\vec{\nabla}P+\eta\nabla^2\vec{v}=\frac{\eta}{\kappa_{GBM}}\vec{v}\ . \tag{3.9}$$

Eq. (3.10) is often employed together with the continuity equation for incompressible fluid;

$$\vec{\nabla}\cdot\vec{v}=0\,. \tag{3.10}$$

จุฬาลงกรณ์มหาวิทยาลัย
CHULALONGKORN UNIVERSITY

The force on a suspending sphere can be found by solving Eq. (3.9) and (3.10) for $\vec{v}$ and P and integrating the hydrodynamic stress over the sphere surface. Because the length of the GBM, L_{GBM}, and the width of the structural unit (W), are both much larger than solute sizes, the GBM is viewed as an unbounded medium. Theoretical analyses by Brinkman (1947) has shown that the force exerted on a sphere moving at velocity $\vec{U}$ in a quiescent fluid ($\vec{F}_t$) and the force on a stationary sphere in a uniform flow $\vec{V}$, $\vec{F}_0$, are

$$\vec{F}_t=-6\pi\eta\vec{U}\left[1+\left(a/\sqrt{\kappa_{GBM}}\right)+\frac{\left(a/\sqrt{\kappa_{GBM}}\right)^2}{9}\right] \tag{3.11a}$$

$$\vec{F}_0 = 6\pi\eta\vec{V}\left[1+\left(a/\sqrt{\kappa_{GBM}}\right)+\frac{\left(a/\sqrt{\kappa_{GBM}}\right)^2}{3}\right] \qquad (3.11b)$$

The convective hindrance factor, K_c, defined as the velocity of a freely-suspending sphere scaled with the unperturbed fluid, $\vec{V}$, can be obtained from the force balance between $\vec{F}_t$ and $\vec{F}_0$ as following;

$$K_c = \frac{U}{V} = \frac{|\vec{F}_0|}{|\vec{F}_t|} = \frac{\left[1+\left(a/\sqrt{\kappa_{GBM}}\right)+\frac{\left(a/\sqrt{\kappa_{GBM}}\right)^2}{3}\right]}{\left[1+\left(a/\sqrt{\kappa_{GBM}}\right)+\frac{\left(a/\sqrt{\kappa_{GBM}}\right)^2}{9}\right]} \qquad (3.12)$$

In our calculation, K_c is calculated by employing Eq. (3.12). The partition coefficient, Φ, is still obtained from the Ogston equation (Eq. (3.8)). It has been reported that the value of the convective permeability, ΦK_c, depends on the pressure applied to the GBM. This dependency has been accounted for by the fact that κ_{GBM} also depends on the applied pressure. At ΔP = 35 mmHg (normal physiological pressure difference), κ_{GBM} = 1-3 nm^2.

จุฬาลงกรณ์มหาวิทยาลัย
Chulalongkorn University

3.4 Intact glomerular basement membrane and cellular blockage

Equation (3.4a) yields θ_{GBM} for solute filtration through an isolated bare GBM. In an *in vivo* glomerular capillary wall, the GBM is not bare but attached to two cellular layers as shown in Fig. (1.4). The equation yielding θ_{GBM} of an intact GBM is modified as following:

$$\theta_{GBM} = \frac{\Phi K_c}{\theta_{ep}\left(1-\exp(-Pe^*)\right)+\Phi K_c \exp(-Pe^*)} \qquad . \qquad (3.13)$$

It is worth noting that the sieving coefficient through the intact GBM also depends on the sieving coefficient through the epithelial cell layer: an evidence that solute transport through the three cell layers influences one another.

To account for the cellular blockage of the GBM, Edwards and colleagues solved Eq. (3.2) but with the surface of the GBM partially blocked by the endothelial cells and the epithelial podocytes, and obtain the correlation between *Pe** shown in Eq. (3.13) and *Pe* in Eq. (3.4a) as following(Edwards et al., 1999):

$$\frac{Pe^*}{Pe} = 1 + 0.7366(1-\varepsilon_f \varepsilon_s)^{11.9864}\left(\frac{L_{GBM}}{W}\right)^{-1.2697} \tag{3.14}$$

Eq. (3.14) accounts for the fact that the fluid flow through the GBM is distorted by the presence of the endothelial and epithelial cell layers. ε_s and ε_f are the GBM surface fractions that are not covered by the podocytes and the endothelial cells, respectively, as defined in Chapter 1. W is the width of the structural unit. In this work, θ_{GBM} of an intact GBM is obtained from Eqs. (3.13) and (3.14) with the diffusive and convective permeabilities calculated as described in Section 3.2 and 3.3. As indicated in Eq. (3.14), in order to determine θ_{GBM}, θ_{ep} has to be obtained first; the procedure of obtaining it was given in the last chapter. In the next section, θ_{GBM} as a function of solute size will be presented for both solute filtration through an isolated and an intact GBM.

จุฬาลงกรณ์มหาวิทยาลัย
Chulalongkorn University

3.5 Results

3.5.1 ΦK_d in the GBM

Shown in Fig. (3.1) is the diffusive permeability of the GBM, ΦK_d, as a function of solute radius (r_s). The lines represent ΦK_d calculated with various combinations of $\phi_{collagen}$ and ϕ_{GAG} under a condition that the total fiber volume fraction = $\phi_{collagen} + \phi_{GAG}$ = 0.1. The steric factor, S, is set at 1 because of GAG flexibility. This is supported by the fact that setting S = 1 had yielded correct diffusivities for spheres suspended in a

dextrin solution. (Dextran is a flexible polymer.) The hydrodynamic factor, F, was calculated using Eq. (3.6a) - (3.6c) by substituting $r_f = r_f^{GAG}$. This is equivalent to assuming that only GAG - macromolecule interaction contributes to the diffusivity reduction. Because $r_f^{collagen}$ is 7 times as large as r_f^{GAG}, equal volume fraction of GAG and collagen in the GBM implies that the number of GAG fibers presented can be as large as 49 times that of collagen fibers. Therefore, it is assumed that the enhanced drag and the solute diffusivity can be calculated by taking into account the GAG-solute interaction alone due to the much higher number of GAG presented in the GBM. The filled circles in Fig. (3.1) are ΦK_d calculated using an empirical expression obtained from an ultrafiltration through an isolated GBM(Bolton et al., 1998). A combination of $\phi_{collagen}$ and ϕ_{GAG} that yields ΦK_d close to the empirical values obtained from ultrafiltration for small and moderate-sized macromolecules is $\phi_{collagen} = \phi_{GAG} = 0.05$ as shown in Fig. (3.1). For larger macromolecules, our calculation underestimates ΦK_d: a trend which can be seen for $r_s > 40$ nm in the figure below.

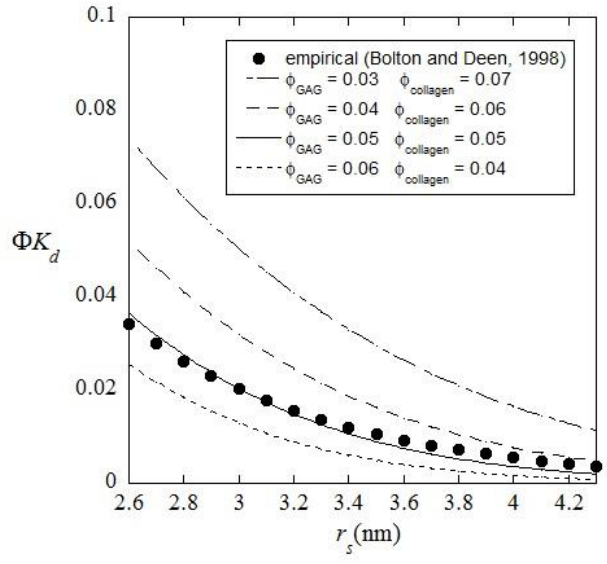

Figure 3.1: Diffusive permeability, ΦK_d, as a function of solute sizes. The calculated results for given values of $\phi_{collagen}$ and ϕ_{GAG} (solid, dashed and dot-dashed lines) are compared with empirical results obtained from ultrafiltration through an isolated GBM (filled circles).

3.5.2 θ_{GBM} through an isolated GBM from calculation and experiments

In Fig. (3.2), θ_{GBM} calculated using Eqs. (3.4a) and (3.4b) with ΦK_d obtained from Eqs. (3.5), (3.6a) - (3.6c) and (3.8) ($\phi_{collagen} = \phi_{GAG} = 0.05$) and ΦK_c from an empirical expression(Bolton et al., 1998) is compared and found to agree well with from θ_{GBM} ultrafiltration through an isolated GBM (filled circles). A conclusion that only GAG-solute interaction contributes to reduction of K_d and protein selectivity, whereas the function of type IV collagen is to maintain the structural integrity, is supported by the fact that mutations in adult type IV collagen leads to distortion of the GBM and a disease called Alport syndrome characterized by only mild proteinuria (Karl Tryggvason & Jorma Wartiovaara, 2005).

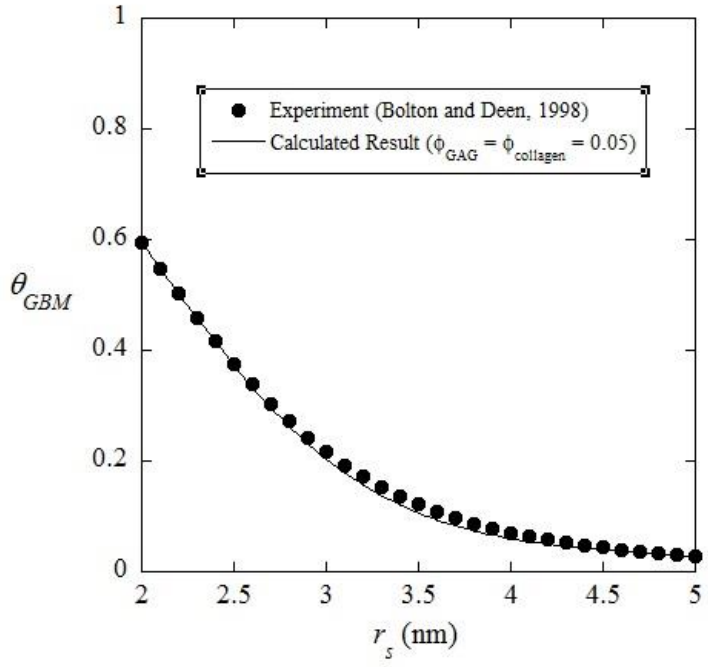

Figure 3.2: Sieving through the glomerular basement membrane, θ_{GBM}, as a function of solute sizes. Calculated results (solid line) are compared with the sieving coefficient calculated from an empirical expression of the diffusive permeability based on experimental results from ultrafiltration through an isolated GBM of Sprague-Drawley rats (filled circles).

As a result, in our work, the diffusive permeability will be calculated with Φ obtained from Eq. (3.8), and K_d obtained from Eq. (3.5) -(3.6c) with only GAG-solute interaction contributes to the factor corresponding to the hydrodynamic effect, F, whereas the steric factor, S, is set at 1. The calculation would be done with $\phi_{collagen}$ = ϕ_{GAG} = 0.05.

3.5.3 θ_{GBM} through an intact GBM

Shown in Figs. (3.3) amd (3.4) are the sieving coefficient through an intact GBM as a function of the solute radii. The physiological parameters employed are that of human: ε_s = 0.086 and ε_f, = 0.2. W, the width of the structural unit, is set at 500 nm, and the GBM thickness is set at 400 nm. The fluid velocity through the GBM is assumed to be 4 μm/s based on a glomerular filtration rate through a single nephron(Edwards et al., 1999).

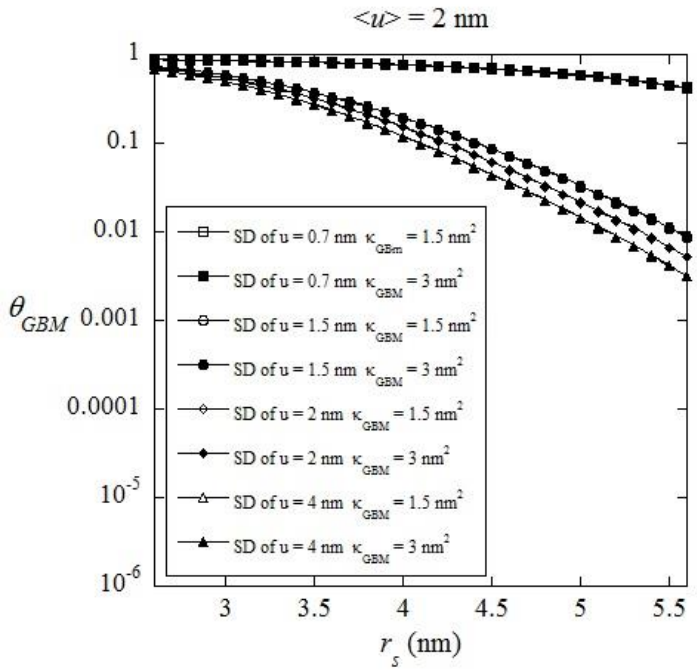

Figure 3.3: θ_{GBM} as a function of r_s. <u> = 2 nm and $\sqrt{\langle u^2 \rangle}$ = 0.7 nm (squares), 1.5 nm (circles), 2 nm (diamonds) and 4 nm (triangles).

As shown in Eq. (3.13), θ_{GBM} is affected by values of θ_{ep}. Shown in Fig. (3.3) is θ_{GBM} with <u> = 2 nm. Results are plotted for various values of $\sqrt{\langle u^2 \rangle}$. As shown in the figure, for the entire range of solute radii presented, θ_{GBM} decreases as $\sqrt{\langle u^2 \rangle}$ increases, indicating that an increase in $\sqrt{\langle u^2 \rangle}$ causes a reduction in θ_{GBM}.

Results plotted in Fig. (3.4) is θ_{GBM} calculated with <u> = 12.10 nm and 22 nm. As shown in the figure below, θ_{GBM} calculated with both values of <u> are very close with θ_{GBM} with <u> = 22 nm being slightly smaller. This is to be expected since θ_{ep} obtained by assuming that <u> = 22 nm is slightly higher. Analogously, θ_{GBM} shown in Fig. (3.4) is smaller than θ_{GBM} shown in Fig. (3.3) due to the values of θ_{ep} calculated with <u> = 2 nm is smaller θ_{ep} calculated with <u> = 12.10 nm and 22 nm that is close to 1. This agrees with results presented in Fig. (4) of Deen et al. (2001) where θ_{GBM} declines as $\theta_{ep} \rightarrow 1$.

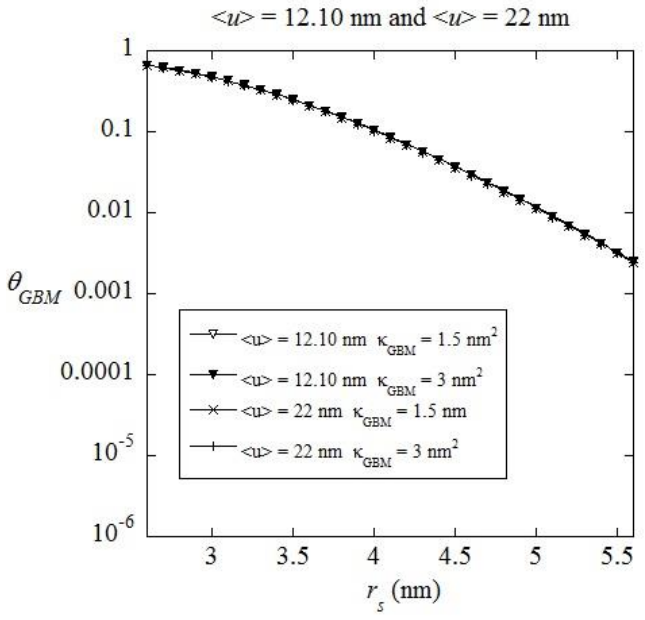

Figure 3.4 : θ_{GBM} as a function of r_s. Results are shown for <u> = 12.10 nm with $\sqrt{\langle u^2 \rangle}$ = 1.39 nm, and <u> = 22 nm with $\sqrt{\langle u^2 \rangle}$ = 4 nm.

It is believed that κ_{GBM} = 1-3 nm^2. More recent estimates has shown that κ_{GBM} = 1.5 nm^2 (Bolton et al., 1998). As shown in both Figs. (3.3) and (3.4), the presented results are from calculations using κ_{GBM} = 1.5 nm^2 (empty symbols) and 3 nm^2 (filled symbols). Values of the calculated θ_{GBM} are very close with the empty symbols and the filled symbols almost completely overlapping. This indicates that θ_{GBM} remains fairly insensitive to the change in κ_{GBM} for the range of values of κ_{GBM} estimated from experiment. In our subsequent calculation, κ_{GBM} is set at 1.5 nm^2.

จุฬาลงกรณ์มหาวิทยาลัย
Chulalongkorn University

Chapter 4
Transport of Macromolecules through the Endothelial Fenestrae

4.1 Application of the steady-state solution of convection-diffusion equation for solute transport in the endothelial cell layer

The endothelial cell layer is full of fenestrae with diameters approximately 50-100 nm(Karl Tryggvason & Jorma Wartiovaara, 2005). Electron microscopy has shown that the fenestrae are filled with GAG-riched glycocalyx. Because the diameters of the fenestrae are much larger than sizes of solutes (proteins), the enhanced drag on the solute due to its interaction with the fenestrae wall is ignored, and we assume that the reduction in diffusivity and the change in convective rate of the solutes are due to its interaction with the GAG that fills the fenestrae alone. The steady-state convection diffusion equation (Eq. (3.2)) becomes one-dimensional, and from its solution, the sieving coefficient through the endothelial cell layer is as following.

$$\theta_{en} = \frac{\Phi_{en} K_c^{en}}{\theta_{GBM}\theta_{ep}\left(1-\exp(-Pe_{en})\right) + \Phi_{en} K_c^{en} \exp(-Pe_{en})} \tag{4.1}$$

where

$$Pe_{en} = \frac{v_{en}\Phi_{en} K_c^{en} L_f}{\Phi_{en} K_d^{en}} \tag{4.2}$$

Due to conservation of mass, v_{en}, the fluid velocity through the fenestrae, is v_{GBM}/ε_f. L_f is the length of the fenestrae. K_d^{en} is calculated the same way as the diffusive hindrance factor of the GBM as stated in Section 3.2 but with the fiber volume fraction, ϕ, being $\phi_{GAG,en}$, the GAG volume fraction within the endothelial fenestrae. K_c^{en} is also calculated as the freely-suspending sphere in a Brinkman medium (Eq. (3.12) but with the Darcy permeability modified to κ_{en}, the Darcy permeability of a gel with random array of cylinders:

$$\kappa_{en} = 0.31\left(r_f^{GAG}\right)^2 \left(\phi_{GAG,en}\right)^{-1.17}. \tag{4.3}$$

The partition coefficient, Φ_{en}, is still calculated using the Ogston equation, but with GAG being the only type of fibers presented as following:

$$\Phi = \exp\left[-\phi_{GAG,en}\left(1+\frac{r_s}{r_f^{GAG}}\right)^2\right] \tag{4.4}$$

Substituting the above parameters into Eq. (4.1) gives us the sieving coefficient through the endothelial cell layer as a function of solute sizes. Because $\phi_{GAG,en}$ is still unknown, it is going to be adjusted until it reaches the value that yield the correct profile of the total glomerular sieving coefficient as a function of solute radii.

4.2 Results: sieving coefficient through the endothelial fenestrae for different volume fraction of GAG

Shown in Fig. 4.1 is the sieving coefficient through an endothelial fenestrae (θ_{en}) as a function of solute radii for $\phi_{GAG,en}$ = 0.06, 0.07, 0.08 and 0.09. The calculation was completed by assuming that <u> = 12.10 nm. As shown in the figure, as $\phi_{GAG,en}$ increases, θ_{en} decreases. It is worth noting that results are shown for two different values of κ_{en}. The solid symbols indicates results calculated employing κ_{en} that was obtained from Eq. (4.3), an expression for a hydraulic permeability of a fibrous media containing rigid uniform-sized fibers(Amsden, 1998). For fluid transport through a media containing flexible fibers in a random array, κ_{en} obtained from Eq. (4.3) should be regarded as a lower bound. There is also another complication: GAG is known to be negatively-charged. Mattern and Deen has demonstrated that the hydraulic permeability through an array of a charged fibers depends on both the fiber charge density, and the concentration of the electrolytic solution(Mattern, 2008). To examine the effect of κ_{en} using in the calculation of K_c^{en} on the sieving coefficient through the endothelial fenestrae, θ_{en} obtained by employing κ_{en} from an expression given by

Amsden (1998) denoted as solid symbols were compared with θ_{en} obtained using κ_{en} = 4.97 nm^2 indicated by the empty symbols. (This value of κ_{en} was estimated from the human glomerular filtration rate of 2.31 nm/s/Pa(Drumond & Deen, 1994).) As shown in the figure, the empty and filled symbols almost overlapped, indicating that θ_{en} is relatively not sensitive to κ_{en} employed in calculating K_c^{en} . For the rest of our calculation, κ_{en} would be obtained by using Eq. (4.3).

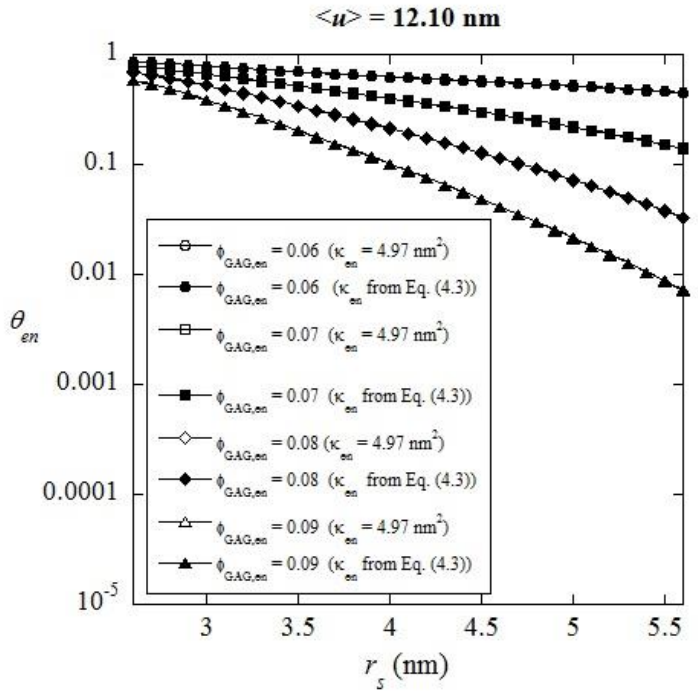

Figure 4.1: Sieving coefficient through the endothelial fenestrae (θ_{en}) as a function of solute radii (r_s) calculated assuming that <u> = 12.10 nm and $\sqrt{\langle u^2 \rangle}$ = 1.39 nm. Results are plotted for $\phi_{GAG,en}$ = 0.06 (circles), 0.07 (squares), 0.08 (diamonds) and 0.09 (triangulars). The employed κ_{en} are 4.97 nm^2 estimated from human glomerular filtration rate (empty symbols) and κ_{en} obtained using Eq. (4.3) (filled symbols).

Not shown in the figure above is the fact that θ_{en} calculated assuming that <u> = 22 nm and $\sqrt{\langle u^2 \rangle}$ = 4 nm based on the observation of Rice et al. (2013) is very close to θ_{en} calculated assuming that <u> = 12.10 nm and $\sqrt{\langle u^2 \rangle}$ = 1.39 nm based on the observation of Gagliardini et al. (2010). For instance, the difference of θ_{en} at r_s = 3.6 nm is less than 1% for all values of $\phi_{GAG,en}$ presented.

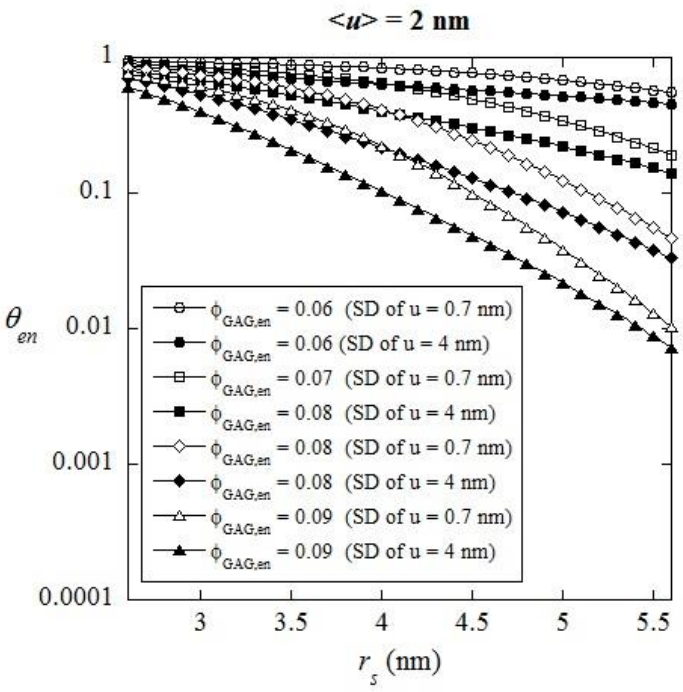

Figure 4.2: Sieving coefficient through the endothelial fenestrae (θ_{en}) as a function of solute radii (r_s) calculated assuming that <u> = 2 nm and $\sqrt{\langle u^2 \rangle}$ = 0.7 nm (empty symbols) and 4 nm (filled symbols). Results are plotted for $\phi_{GAG,en}$ = 0.06 (circles), 0.07 (squares), 0.08 (diamonds) and 0.09 (triangulars).

Different values of θ_{en} were obtained, however, if the calculation was done assuming that $<u>$ = 2 nm. As shown in Fig. (4.2), θ_{en} decreases as the standard deviation of u increases from 0.7 nm to 4 nm. This is because, similarly to the fact that θ_{GBM} decreases as θ_{ep} increases, an increase in the product of θ_{GBM} and θ_{ep} would causes a reduction in θ_{en} as shown above.

After the sieving coefficient through all three cellular layers were obtained, the total glomerular sieving coefficient could be obtained as their product as will be discussed in the next chapter.

จุฬาลงกรณ์มหาวิทยาลัย
Chulalongkorn University

Chapter 5
Total Glomerular Sieving Coefficient

After the sieving coefficients through the endothelial cell layer (θ_{en}) , the GBM (θ_{GBM}) and the epithelial cell layer (θ_{ep}) were determined, the total glomerular sieving coefficient (θ) can be calculated by using the definition that the overall glomerular sieving coefficient is simply the product of the sieving coefficient of the three layers as shownin Eq. (1.8). The methodology employed in obtaining the total glomerular sieving coefficient is reviewed in Sect. 5.1. Then, in Sect. 5.2, the calculated result was compared with the sieving coefficient of ficoll (highly cross-linked polysaccharide that is spherical, uncharged and not absorbed in the glomerular tubule) obtained from *in vivo* urinalnalysis.

5.1 Methodology

The summary of the calculation of the total glomerular sieving coefficient is presented in the form of a flow chart as shown in Fig. (5.1). First, the epithelial slit is modeled as a row of parallel cylinders with non-uniform spacing. The sieving coefficient through the epithelial cell layer was determined as the averaged sieving coefficient through the slit diaphragm by employing the expression shown in Eq. (2.11). The dimensionless flow resistance was calculated by solving the Stokes and continuity equations using finite element method, whereas the distribution function of half-spacing between cylinders were obtained from electron microscopy. The epithelial slit radius is set at 6.5 nm (estimated from images from observations of Rice et al. (2013)). The sieving coefficient through the GBM and the endothelial fenestrae were calculated from an analytical solution of the one-dimensional pseudo-steady convection-diffusion equation with the diffusive and convective hindrance factors obtained from applications of existing theory for transport in fibrous media. After the sieving coefficient through the three layers were determined, the total sieving coefficient, the product of the sieving

coefficient of the three layers, would be compared to sieving coefficient of ficoll obtained from *in vivo* urinalysis in human.

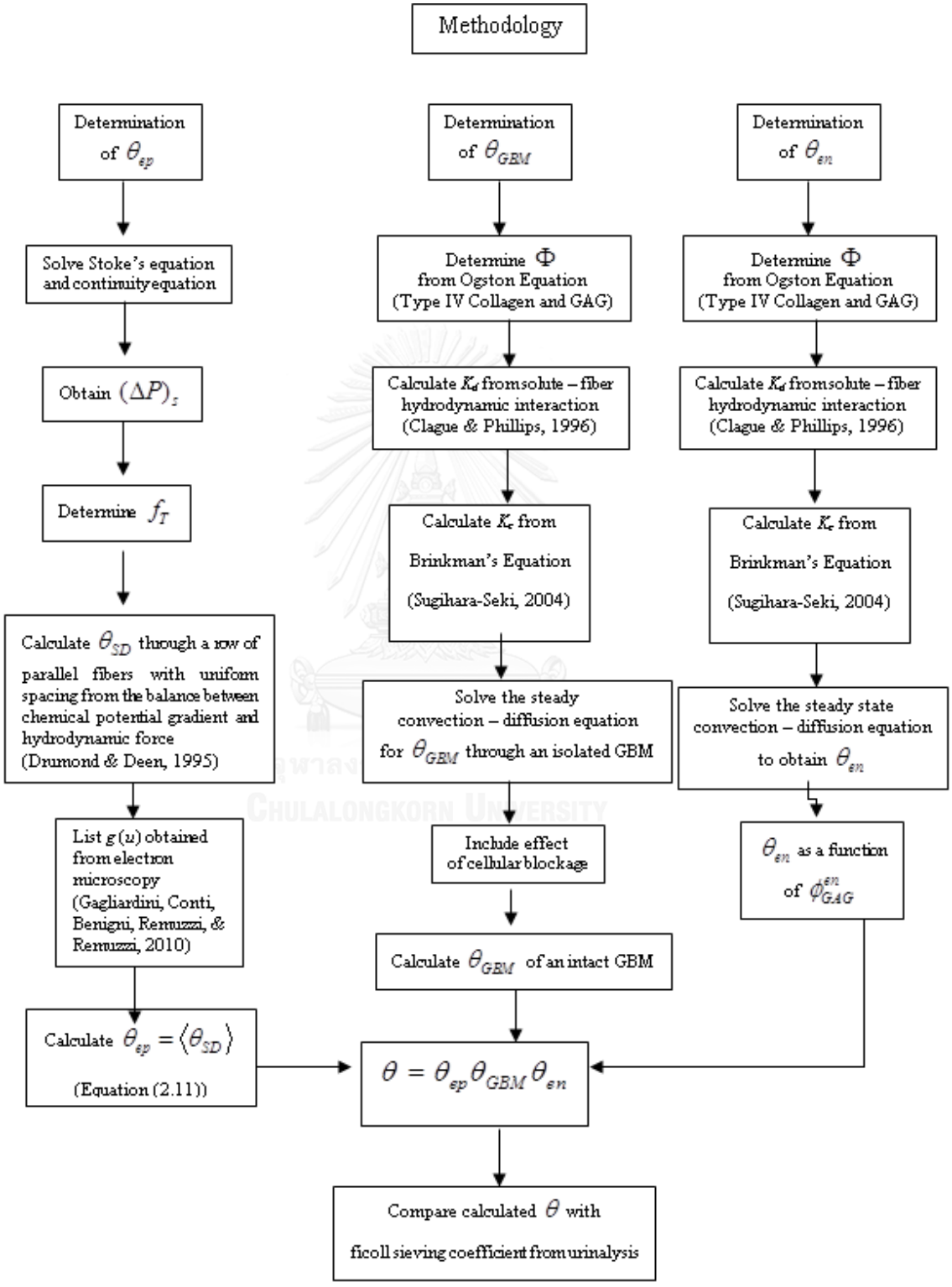

Figure 5.1 Flowchart of determination of total glomerular sieving coefficient

5.2 Results : total sieving coefficient

5.2.1 <*u*> = 12 nm and 22 nm

Shown below in Figs. (5.2) and (5.3) is the comparison between our calculated results for sieving of electrically neutral sphere through the glomerular barrier and ficoll sieving obtained from *in vivo* urinalysis for humans. Results in Figs. (5.2) and (5.3) were completed by assuming that <*u*> = 12 nm and 22 nm, respectively. As shown in the figures, the total sieving coefficients obtained by assuming that <*u*> = 12 nm is very close to that obtained by assuming that <*u*> = 22 nm due to their very close values of θ_{ep}. As expected, the total sieving coefficient decreases when the volume fraction of GAG in the endothelial fenestrae increases. As shown in both figures, our calculated results agree very well with the experimental data for human glomerular capillary wall when the volume fraction of GAG in the endothelial fenestrae, $\phi_{GAG,en}$, is 0.07. In estimating the contribution of each cellular layer to glomerular size-selectivity (Fig. (5.5)), $\phi_{GAG,en}$ is set at 0.07.

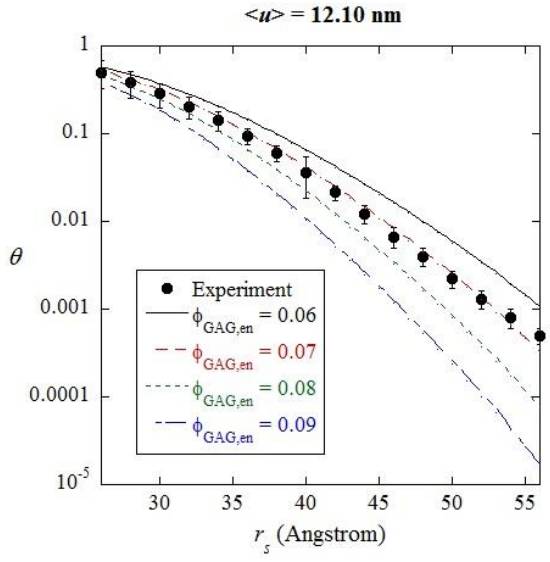

Figure 5.2: θ as a function of r_s for $\phi_{GAG,en}$, being 0.06 (solid line), 0.07 (red dashed line), 0.08 (green dashed line) and 0.09 (blue dot dashed line) calculated with <*u*> = 12.10 nm. Also presented is experimental data of ficoll sieving from *in vivo* urinalysis in human (Blouch et al., 1997).

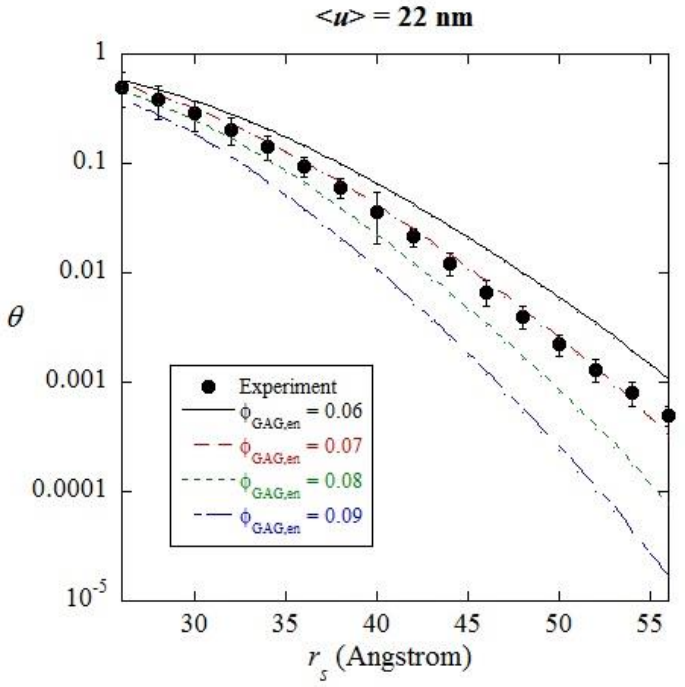

Figure 5.3: θ as a function of r_s for $\phi_{GAG,en}$, being 0.06 (solid line), 0.07 (red dashed line), 0.08 (green dashed line) and 0.09 (blue dot dashed line) calculated with <*u*> = 22 nm. Also presented is experimental data of ficoll sieving from *in vivo* urinalysis in human (Blouch et al., 1997).

จุฬาลงกรณ์มหาวิทยาลัย
Chulalongkorn University

In Fig. (5.4), the total sieving coefficient and the sieving coefficient through each cellular layer are presented as functions of solute radii for healthy humans. Experimental results from urinalnalysis are also presented. With the averaged half gap-width between adjacent fibers in the slit diaphragm being 12 nm (more than 2 times larger than the radius of the largest test solute), the slit diaphragm almost does not restrict solute transport. θ_{ep} is close to 1. For transport through human glomerular barrier, θ_{GBM} is the smallest sieving coefficient for the entire range of solute radii presented.

In Fig. (5.5), the calculated sieving of electrically neutral sphere through the glomerular barrier is shown as a function of solute radii under an assumption that <*u*> = 22 nm and $\sqrt{\langle u^2 \rangle}$ = 4 nm. The contribution of each layer to solute restriction is similar to the calculation completed by assuming that <*u*> = 12 nm as shown earlier in Figs. (5.4), despite the almost two-times difference in the reported values of <*u*> between the observations of Gagliardini et al. (2010) and Rice et al. (2013). For both values of <*u*>, θ_{ep} is close to 1 due to the fact that <*u*> is several times larger than solute radii. Because the slit diaphragm does not restrict solute transport, the total sieving is simply the product of the GBM and the endothelial cell layer.

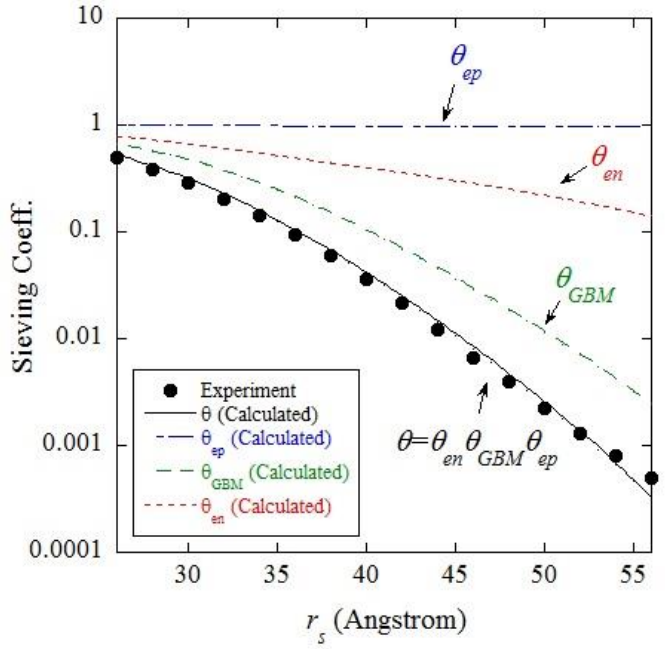

Figure 5.4: Calculated total sieving coefficient (black solid line) as well as sieving coefficients through the epithelial cell layer (blue dot dashed line), the GBM (green dashed line) and the endothelial cell layer (red dashed line) as functions of solute radii. <*u*> = 12 nm. Also presented is the sieving coefficient of ficoll (filled circles) from *in vivo* urinalysis experiment(Blouch et al., 1997).

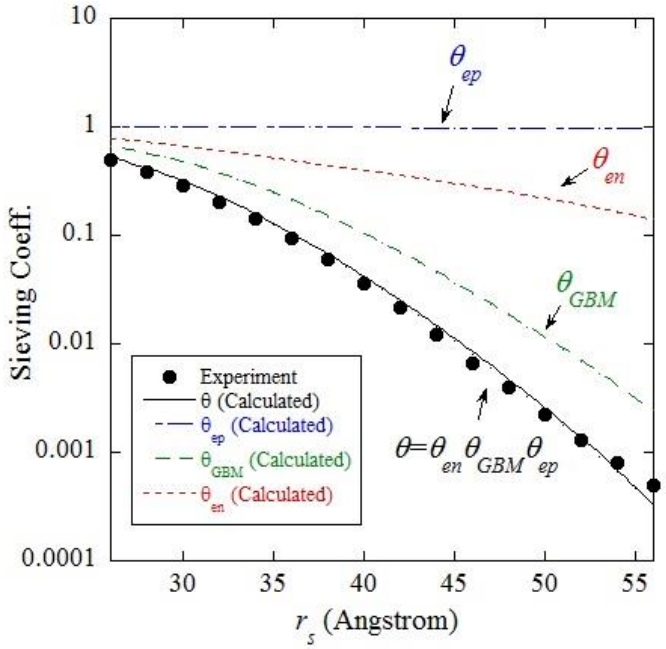

Figure 5.5: Calculated total sieving coefficient (black solid line), and sieving coefficients through the epithelial cell layer (blue dot dashed line), the GBM (green dashed line) and the endothelial cell layer (red dashed line) as functions of solute radii. $\langle u \rangle$ = 22 nm. Also presented is the sieving coefficient of ficoll (filled circles) *in vivo* urinalnalysis in human (Blouch et al., 1997).

จุฬาลงกรณ์มหาวิทยาลัย
Chulalongkorn University

By employing the recent dimensions of the gap-width of slit diaphragm from scanning electron microscopy and helium ion scanning microscopy, our calculation has shown that the endothelial cell layer and the GBM contribute significantly to solute restriction of the glomerular barrier. Traditionally believed to contribute significantly to glomerular charge selectivity, our results indicate that the glycocalyx-filled endothelial fenestrae can contribute significantly to glomerular size-selectivity as well. This is supported by data of experiments performed in rodents: Jeansson and Haraldsson has shown that the sieving coefficient of ficolls from urinalysis and cool perfused isolated kidney experiments increased in mice exposed to GAG-degrading enzymes despite ficolls being electrically neutral(Jeansson & Haraldsson, 2003).

The fact that θ_{ep} is close to 1 in the calculation indicating that the slit diaphragm does not restrict solutes seems to be in contradiction with reports of patients with nephrotic syndrome of the Finnish type exhibiting both the loss of the slit diaphragm and proteinuria. However, several studies also demonstrated that proteinuria may occur without effacement of podocyte foot process(Haraldsson et al., 2008) or the damage to the slit diaphragm, such as proteinuria observed in patients with pre-eclampsia and early diabetes. A close inspection of an image of the slit diaphragm from helium ion microscopy of Rice et al. (2013) reveals another structure underneath the first cross-bridging filaments. It is possible that that structure is the GBM as speculated by Rice et al. (2013), or as proposed by Wartiovaara et al. (2004) from electron tomography, the second layer of the slit diaphragm(Wartiovaara et al., 2004). Further investigation about the slit diaphragm structure, such as images from transmission electron microscopy with higher resolution than that employed by Rodewald and Karnovsky (1974), is still needed.

5.2.2 $<u>$ = 2 nm

To examine the implication of the slit diaphragm having smaller $<u>$ as reported by Rodewald and Karnovsky (1974) and Wartiovaara et al. (2004) (possibly due to the fact that the smaller $<u>$ is the half-width of the gap where the two layers of the slit diaphragm are not overlapping, although as aforementioned, a confirmation from TEM with higher resolution is still needed.), the sieving coefficient calculated by assuming that $<u>$ = 2 nm with $\sqrt{<u^2>}$ being 0.7, 1.5, 2, 3 and 4 nm is plotted as a function of solute radii. Results shown in Fig. (5.5) is calculated by assuming that only the GBM and the epithelial cell layer contributes to solute restriction, whereas the contribution of the endothelial cell layer is neglected. As shown in the figures, the sieving coefficient increases as $\sqrt{<u^2>}$ increases. However, none of the $\sqrt{<u^2>}$ presented yields the sieving coefficient that agrees with sieving coefficient of ficoll obtained from urinalysis in human. The percentage of discrepancy is especially large for larger solutes.

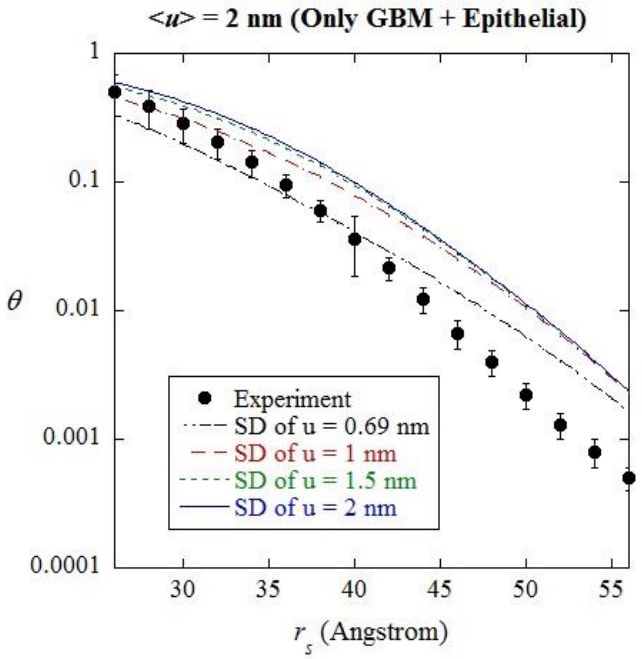

Figure 5.6: Calculated total sieving coefficient as functions of solute radii. <*u*> = 2 nm. Results are plotted for $\sqrt{\langle u^2 \rangle}$ = 0.69 nm (dot-dashed line), 1 nm (dashed line), 1.5 nm (dashed line) and 2 nm (solid line). Also presented is the sieving coefficient of ficoll (filled circles) from *in vivo* urinalysis experiment (Blouch et al., 1997).

To examine the effect of including the contribution of the endothelial cell layer to solute restriction, the total sieving coefficients calculated for $\phi_{GAG,en}$ = 0.06 - 0.09 are shown in Figs. (5.7) - (5.9). Results calculated by assuming that <*u*> = 2 nm and $\sqrt{\langle u^2 \rangle}$ = 0.7 nm are plotted as functions of solute radii in Fig. (5.7). Once again, as $\phi_{GAG,en}$ increases, θ decreases. The lowest difference between the calculated sieving coefficient and the experimental result from urinalysis is obtained when $\phi_{GAG,en}$ is set at 0.07, where the percentage of discrepancy is lowered significantly (compared to results shown in Fig. (5.6)) for solute with larger radii, although the percentage of discrepancy is still large for smaller solutes.

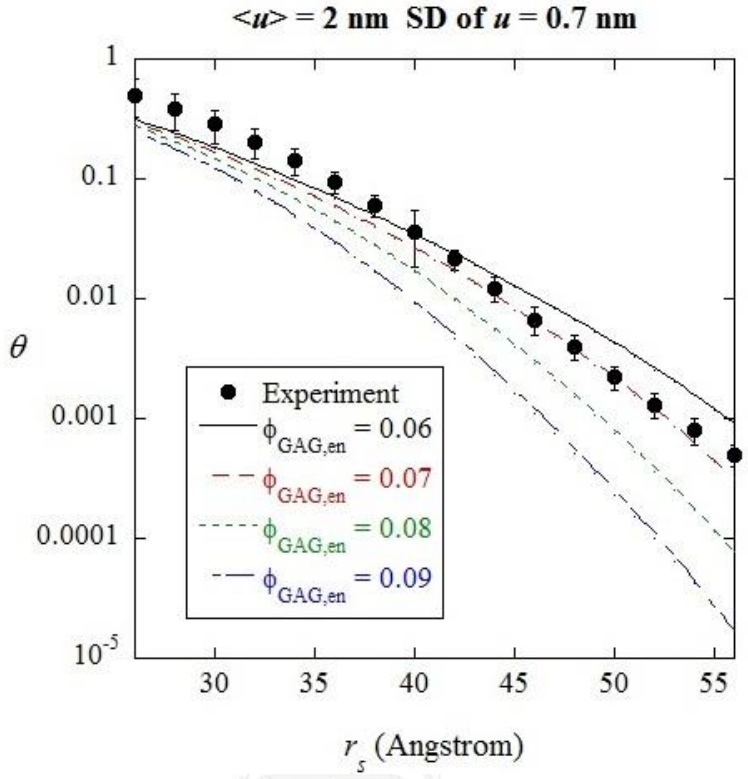

Figure 5.7: Total sieving coefficient as a function of solute radii. <*u*> = 2 nm and $\sqrt{\langle u^2 \rangle}$ = 0.7 nm. Results are calculated by setting $\phi_{GAG,en}$ at 0.06 nm (solid line), 0.07 (dashed line), 0.08 (dashed line) and 0.09 (dot-solid line). Also presented is the sieving coefficient of ficoll (filled circles) from *in vivo* urinalysis experiment (Blouch et al., 1997).

Shown in Figs. (5.8) and (5.9) are sieving coefficient calculated by assuming that <*u*> = 2 nm and $\sqrt{\langle u^2 \rangle}$ = 1, 2 and 4 nm, respectively. For all values of $\sqrt{\langle u^2 \rangle}$ presented, the percentage of discrepancy between the calculated sieving coefficient and the sieving coefficient of ficolls from urinalysis is lowest when $\phi_{GAG,en}$ = 0.07. It can be seen from the figures that the difference between the calculated sieving coefficient and the sieving coefficient of ficolls from urinalysis that is more noticeable for smaller

solute is lowered as $\sqrt{\langle u^2 \rangle}$ (and hence, θ_{ep}) increases. As shown below in Fig. (5.9), calculations done by assuming that $\sqrt{\langle u^2 \rangle}$ = 2 nm and 4 nm and $\phi_{GAG,en}$ = 0.07 yield the sieving coefficient that agrees very well with the experimental result.

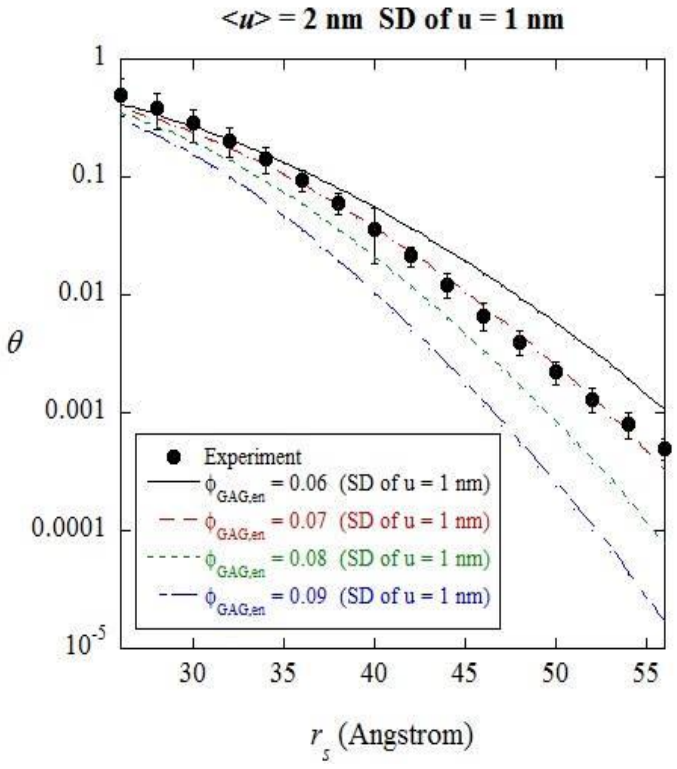

Figure 5.8: Total sieving coefficient as a function of solute radii. <*u*> = 2 nm and $\sqrt{\langle u^2 \rangle}$ = 1 nm. Results are calculated by setting $\phi_{GAG,en}$ at 0.06 nm (solid line), 0.07 (dashed line), 0.08 (dashed line) and 0.09 (dot-solid line). Also presented is the sieving coefficient of ficoll (filled circles) from *in vivo* urinalysis experiment (Blouch et al., 1997).

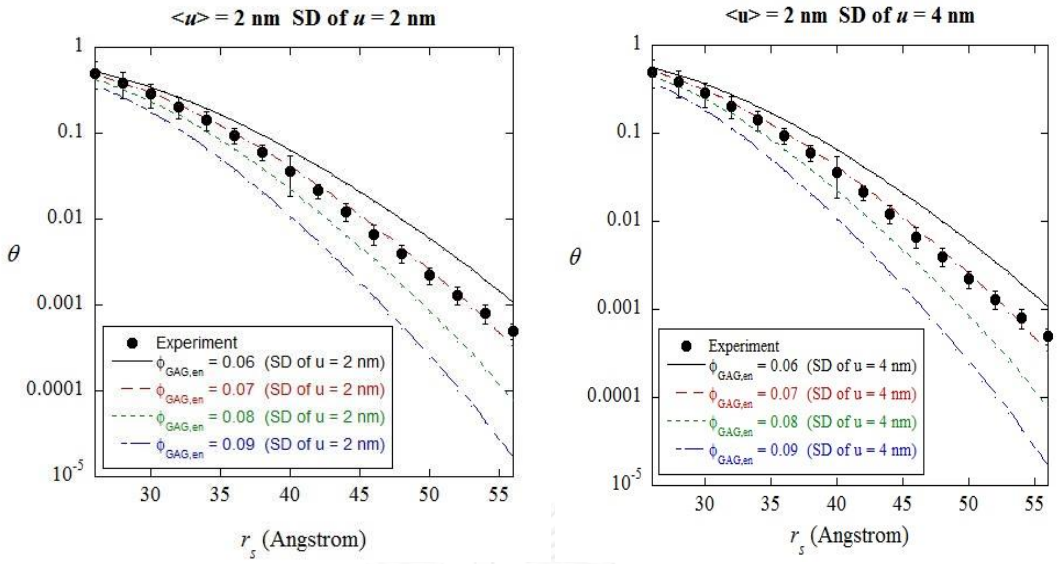

Figure 5.9: Total sieving coefficient as a function of solute radii. <*u*> = 2 nm and $\sqrt{\langle u^2 \rangle}$ = 2 nm (left) and 4 nm (right). Results are calculated by setting $\phi_{GAG,en}$ at 0.06 nm (solid line), 0.07 (dashed line), 0.08 (dashed line) and 0.09 (dot-solid line). Also presented is the sieving coefficient of ficoll (filled circles) from *in vivo* urinalysis experiment (Blouch et al., 1997).

Shown in Fig. (5.10) are the total sieving coefficient and the sieving coefficient through each layer as a function of solute radii. The calculation was done by assuming that <*u*> = 2 nm, whereas $\sqrt{\langle u^2 \rangle}$ is set at 2 nm (dashed line) and 4 nm (solid line) which, as shown above in Fig. (5.9), yield the sieving coefficient that agrees well with experimental result. The trend shown below in Fig. (5.10) is quite similar to the trend shown in Figs. (5.4) and (5.5). The epithelial (although not as close to 1 as θ_{ep} shown in Figs. (5.4) and (5.5)) is larger than θ_{en} and θ_{GBM}. As shown in the figure, the GBM plays a crucial role in glomerular restriction. Traditionally believed to contribute majorly to glomerular charge selectivity, the contribution of the endothelial cell layer to size-selectivity is also shown to be significant.

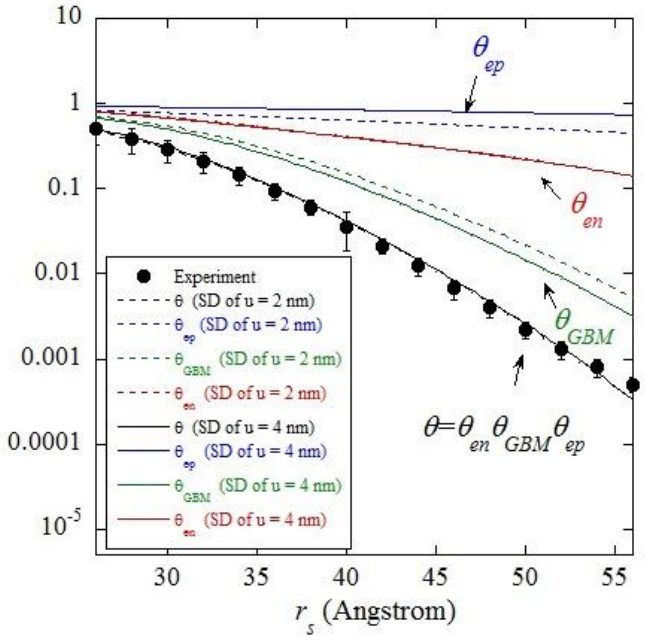

Figure 5.10: Calculated total sieving coefficient (black lines), and sieving coefficients through the epithelial cell layer (blue lines), the GBM (green lines) and the endothelial cell layer (red lines) as functions of solute radii. The calculation was done by assuming that <*u*> = 2 nm, whereas $\sqrt{\langle u^2 \rangle}$ = 2 nm (dashed lines) and 4 nm (solid lines). Also presented is the sieving coefficient of ficoll (filled circles) *in vivo* urinalnalysis in human (Blouch et al., 1997).

จุฬาลงกรณ์มหาวิทยาลัย
Chulalongkorn University

5.3 Conclusion

Calculated total glomerular sieving coefficient agrees very well with the experimental data for human glomerular capillary wall when the volume fraction of GAG in the endothelial fenestrae, $\phi_{GAG,en}$, is 0.07. From Figs. (5.4) and (5.5), if the half-spacing between fibers in the epithelial slit follows the log-normal distribution with <*u*> = 12.10 nm and 22 nm based on the recent observation of Gagliardini et al (2010) and Rice et al. (2013), it is found that the GBM and the endothelial cell layer are the most important layers in solute transport restriction in glomerular filtration, whereas the contribution of the epithelial cell layer can be neglected. If *u*, instead, is assumed

to follow the log-normal distribution with <u> = 2 nm, at values of $\sqrt{\langle u^2 \rangle}$ that yields the sieving coefficient which agrees well with experimental result, a similar trend is also observed. The GBM and the endothelial cell layer play crucial roles in glomerular size-selectivity, whereas, although θ_{ep} is not as small as that calculated by assuming that <u> = 12.10 or 22 nm, it is still significantly larger than θ_{GBM} and θ_{en}. The fact that the endothelial cell layer also contributes to the barrier's size-selectivity is supported by the experiment of Jeansson and Haraldsson (2003) where the sieving coefficient of ficolls from urinalysis and cool perfused isolated kidney experiments increased in mice exposed to GAG-degrading enzymes.

จุฬาลงกรณ์มหาวิทยาลัย
Chulalongkorn University

Chapter 6
Fluid Transport through Fibrous Media and a Row of Parallel Fibers: Applications to Glomerular Filtration

As discussed earlier in Section 1.3, the contribution to the total glomerular hydraulic permeability (k) of the endothelial cell layer (k_{en}), the GBM (k_{GBM}) and the epithelial cell layer (k_{ep}) is given in Eq. (1.4). In this chapter, the calculation of k_{ep}, k_{GBM} and k_{en} based on available physiological information will be stated in details. The relative contribution to fluid restriction of each layer will be discussed. The calculated total glomerular hydraulic permeability will be compared with glomerular hydraulic permeability obtained from micropuncture experiment performed on rats and estimated from glomerular filtration rate in humans.

6.1 Averaged hydraulic permeability through the epithelial slit ($<k_s>$)

6.1.1 Fluid transport through a row of parallel fiber with non-uniform spacing

As aforementioned, the slit diaphragm in the epithelial cell layer of the glomerular capillary wall is modeled as a row of parallel fibers attached to parallel walls with the spacing between adjacent fibers follow either the log-normal or gamma distribution. If *g (u)* is the distribution function of the fiber spacing, an averaged velocity can be calculated using a following equation:

$$< V_s >= \frac{\int_0^\infty (u+R)g(u)V_s du}{\int_0^\infty (u+R)g(u)du} \tag{6.1}$$

where $<V_s>$ is an averaged fluid velocity. u is the half-width of the gaps between adjacent fibers, whereas R is the fiber radius of the slit diaphragm. V_s is the fluid velocity in the slit channel. The distance between the centerlines of two adjacent fibers equals $u + R$.

An averaged hydraulic permeability, a ratio between the averaged velocity and the pressure difference, can be written as following:

$$< k_s >= \frac{< V_s >}{(\Delta P)_s} = \frac{\int_0^\infty (u+R) g(u) V_s du}{(\Delta P)_s \int_0^\infty (u+R) g(u) du} \tag{6.2}$$

where $<k_s>$ is an averaged hydraulic permeability and $(\Delta P)_s$ is the pressure drop across the epithelial slit. There exists previous calculation involving the relationship between the velocity, V_s, and the pressure drop, $(\Delta P)_s$, in a form of the dimensionless flow resistance, f_T , defined as

$$f_T = \frac{(u+R)(\Delta P)_s}{\eta V_s} \tag{6.3}$$

η is the fluid viscosity. Combining equations (6.2) and (6.3), the relationship between hydraulic permeability and dimensionless flow resistance becomes

$$< k_s >= \frac{\int_0^\infty (u+R)^2 f_T^{-1} g(u) du}{\eta \int_0^\infty (u+R) g(u) du} \tag{6.4}$$

The detailed calculation of f_T is given in section 2.2.3. Once both f_T and g (u) are obtained, the averaged hydraulic permeability of the epithelial slit can be determined as will be discussed below.

6.1.2 Possible distribution functions of fiber spacing of the slit diaphragm

As discussed in Chapter 2, our assumption is that the distribution function of u, the half-width of the spacing between adjacent fibers of the slit diaphragm, follows either the gamma distribution or the lognormal distribution:

$$g_{gamma}(u) = \frac{\gamma_2^{\gamma_1} u^{\gamma_1 - 1} e^{-\gamma_2 u}}{\Gamma(\gamma_1)} \tag{6.5}$$

$$g_{\log normal}(u) = \frac{1}{u\sigma\sqrt{2\pi}} e^{-\frac{(\ln u-\mu)^2}{2\sigma^2}} \tag{6.6}$$

where γ_1, γ_2, μ and σ are all constants, and $\Gamma(\gamma_1)$ is the gamma function of γ_1 . If $g(u)$ is the gamma distribution, the mean and variance of u, $<u>$ and $<u^2>$, can be calculated from the values of γ_1 and γ_2 as shown below.

$$< u >_{gamma} = \frac{\gamma_1}{\gamma_2} \tag{6.7a}$$

$$< u^2 >_{gamma} = \frac{\gamma_1}{\gamma_2^2} \tag{6.7b}$$

If $g(u)$ is the log-normal distribution, the mean and variance of u, $<u>$ and $<u^2>$, can be calculated from the values of μ and σ as following.

$$< u >_{\log normal} = e^{\mu+\frac{\sigma^2}{2}} \tag{6.8a}$$

$$< u^2 >_{\log normal} = (e^{\sigma^2} - 1)e^{2\mu+\sigma^2} \tag{6.8b}$$

The standard deviation of u is simply the square root of the variance given in equation (6.7b) and (6.8b).

As mentioned earlier, from SEM observation, Remuzzi et al. (2010) claimed that the sizes of the voids in the slit diaphragm follows a log-normal distribution with $<u>$ = 12.10 nm and $\sqrt{\langle u^2 \rangle}$ = 1.389 nm for Wistar rats. For Munich-Wistar Fromter rats, $<u>$ = 11.42 nm whereas $\sqrt{\langle u^2 \rangle}$ was similar to that of the slit diaphragm of Wistar rats. Rice et al. (2013) employed high resolution helium ion scanning electron microscopy, and found that the sizes of u are larger at 22 ± 8 nm. Values of μ and σ can be obtained from Eqs. (6.8a) and (6.8b) as shown below in Table 3.1. If both $g(u)$ and f_T are determined, $<k_s>$ can be calculated from Eq. (6.4)

It is worth noting that, apart from obtaining $<k_s>$ from the known distribution function, $g(u)$, if instead, $<k_s>$ and the solute sieving coefficient are known, it is possible to determine $g(u)$ using the Newton-Raphson method. Details are given in Appendix A.

6.1.3 Calculated averaged hydraulic permeability of the slit diaphragm

Shown in Table 6.1 is the calculated $<k_s>$ where $g(u)$ is assumed to follow the log-normal distribution and R = 4.5 nm . $<k_s>$ is 682 nm/s/Pa for Wistar rats (with $<u>$ = 12.10 nm), and slightly lower at 650 nm/s/Pa for Munic-Wistar Fromter rats (with $<u>$ = 11.42 nm), resulting in k_{ep} = 75 and 71.5 nm/s/Pa. If $<u>$ is 22 nm and $\sqrt{\langle u^2 \rangle}$ = 4 nm, according to results of Rice et al. (2013), $<k_s>$ becomes 976 nm/s/Pa and k_{ep} = 107.36 nm/s/Pa.

Table 6.1: Averaged hydraulic permeability of the slit diaphragm ($<k_s>$) with R = 4.5 nm ,ε_s (uncovered GBM surface fraction) = 0.11 and $g(u)$ follows the log-normal distribution

Types of rats	Parameters from SEM observation		$<k_s>$ (nm/s/Pa)	$k_{ep} = \varepsilon_s < k_s >$ (nm/s/Pa)
	$<u>$ (nm)	$\sqrt{\langle u^2 \rangle}$ (nm)		
Wistar*	12.10	1.389	682	75
Munich Wistar Fromter*	11.42	1.389	650	71.5
Sprauge-Dawley**	22	4	976	107

* Results of Gagliardini et al. (2010) ** Results of Rice et al. (2013)

If we are to assume that $g(u)$ of human slit diaphragm also follows the very same log-normal distribution but with larger R at 6.5 nm (which yields the correct sieving coefficient), the calculated $<k_s>$ is given in Table 6.2.

Table 6.2: Averaged hydraulic permeability of the slit diaphragm (<k_s>) with R = 6.5 nm, ε_s = 0.086 and g (u) follows the log-normal distribution

Parameters from SEM observation		<k_s> (nm/s/Pa)	$k_{ep} = \varepsilon_s < k_s >$ (nm/s/Pa)
<u> (nm)	$\sqrt{\langle u^2 \rangle}$ (nm)		
12.10	1.389	1,278	110
11.42	1.389	1,205	104
22	4	2,023	174

To examine how different types of g (u) affect <k_s>, the averaged hydraulic permeability of the slit diaphragm calculated with g (u) following the gamma distribution is given below in Table 6.3 (R = 4.5 nm) and Table 6.4 (R = 6.5 nm). It was found that k_{ep} obtained by assuming that g (u) follows the gamma distribution was equal to k_{ep} calculated under an assumption that g (u) is the log-normal distribution.

Table 6.3: Averaged hydraulic permeability of the slit diaphragm (<k_s>) with R = 4.5 nm, ε_s = 0.11 and g (u) follows the gamma distribution

Parameters from SEM observation		Parameters in Equation (6.5)		<k_s> (nm/s/Pa)	$k_{ep} = \varepsilon_s < k_s >$ (nm/s/Pa)
<u> (nm)	$\sqrt{\langle u^2 \rangle}$ (nm)	γ_1	γ_2 (nm^{-1})		
12.10	1.389	75.89	6.272	682	75
11.42	1.389	67.60	5.919	650	71.5
22	4	30.25	1.375	976	107

Table 6.4: Averaged hydraulic permeability of the slit diaphragm (<k_s>) with R = 6.5 nm, ε_s = 0.086 and g (u) follows the gamma distribution

Parameters from SEM observation		Parameters in Equation (6.5)		<k_s> (nm/s/Pa)	$k_{ep} = \varepsilon_s < k_s >$ (nm/s/Pa)
<u> (nm)	$\sqrt{\langle u^2 \rangle}$ (nm)	γ_1	γ_2 (nm^{-1})		
12.10	1.389	75.89	6.272	1,278	110
11.42	1.389	67.60	5.919	1,205	104
22	4	30.25	1.375	2,023	174

Results of Gagliardini et al. (2010) and Rice et al. (2013) are contradictory to earlier results of Rodewald and Karnovsky (1974) using TEM, and that of Wartiovaara et al. (2004) obtained from electron tomography where <u> is approximately 2 nm. If one is to use that value of <u>, and set $\sqrt{\langle u^2 \rangle}$ at 1.5 nm, <k_s> is found at 83 nm/s/Pa (in rats) or 118 nm/s/Pa (in humans) and k_{ep} = 9 and 10 nm/s/Pa, respectively.

6.2 Hydraulic permeability of the endothelial cell layer (k_{en})

As discussed in Section 1.2, the endothelial cell layer consists of a large number of fenestrae filled with glycocalyx believed to be composed majorly of sulfated proteoglycans and glycoprotein. Proteoglycan consists of a core protein and one or more GAG chains. If we are to assume that the major contribution to fluid restriction of the endothelial cell layer, the Darcy permeability of the endothelial fenestrae (κ_f) can be calculated using the expression obtained by Amsden (1998) (Eq. (4.3)) with r_f = 0.5 nm and found to be 1.74 nm^2 for the volume of GAG inside the fenestrae, ϕ_{GAG}^{en}, being 0.07. The relationship between the fenestrae hydraulic permeability (k_f) and the Darcy permeability (κ_f) of the filling inside the endothelial fenestrae can be written as following:

$$k_f = \frac{\kappa_f}{\eta L_{en}} \tag{6.9}$$

Using equation (6.9) with κ_f = 1.74 nm^2, η (the water viscosity at 37 °C) = 8.9 x 10^{-4} Pa.s and L_{en} (the length of the fenestrae) = 70 nm, k_f = 35.5 nm/s/Pa for ϕ_{GAG}^{en} = 0.07. Deen et al. (2001) has calculated k_f of for empty fenestrae and found it to be 100 nm/s/Pa. Therefore, the presence of GAG with ϕ_{GAG}^{en} = 0.07 decreases k_f more than 50%. Because $k_{en} = \varepsilon_f k_f$, it is estimated that k_{en} = 7.1 nm/s/Pa.

6.3 Hydraulic permeability of the glomerular basement membrane (k_{GBM})

As aforementioned, the glomerular basement membrane (GBM) of the glomerular capillary wall is a hydrogel containing several types of protein fibers. Experiments conducted in order to determine a hydraulic permeability of an isolated GBM has shown that k_{GBM} did depend on the applied pressure. With the applied pressure being 35 mmHg (physiological value), the Darcy permeability (κ_{GBM}) was reported at 1-3 nm^2 (Deen et al., 2001; Edwards et al., 1997). Drumond and Deen determined the relationship between k_{GBM} and κ_{GBM} using the continuity equation ($\nabla \cdot \vec{v} = 0$), assuming that there was no transcellular flow and the streamlines of the filtrated fluid were distorted by the endothelium cells and the podocytes(Drumond & Deen, 1994). The expression they obtained is

$$k_{GBM} = \frac{\kappa_{GBM}}{\eta L_{GBM}} \left[1 + \frac{W}{\pi L} \left\{ \frac{1}{n_f} \left[\frac{3}{2} - \ln\left(2\pi\varepsilon_f\right) \right] + \frac{3}{2} - \ln(2\pi\varepsilon_s) \right\} \right]^{-1} \qquad (6.10)$$

The definitions and the values of parameters shown in Eq. (6.10) are given in Chapter 3. n_f is the number of fenestrae per structural unit believed to be 3.

จุฬาลงกรณ์มหาวิทยาลัย
CHULALONGKORN UNIVERSITY

6.4 Total glomerular hydraulic permeability

Shown Below is the total hydraulic permeability, *k*, calculated by using Eq. (1.4) as well as the hydraulic permeability of each cellular layer. If we are to assume that $g(u)$ of rats and human is similar, , *k* as well as k_{ep}, k_{GBM} and k_{en} in the case of healthy human is given below in Table 6.6. ϕ_{GAG}^{en} = 0.07 and $g(u)$ follows the log-normal distribution. It can be seen that the most restrictive layer (in terms of fluid transport) is the GBM. The endothelial cell layer also contributes significantly to fluid restriction, whereas the contribution of the epithelial cell layer depends on the mean and the standard deviation of *u*.

Table 6.5: k and the hydraulic permeability of each cellular layer in healthy human.

κ_{GBM} = 1.5 nm^2. R = 6.5 nm

Parameters from SEM and TEM observation		k_{ep} (nm/s/Pa)	k_{GBM} (nm/s/Pa)	k_{en} (nm/s/Pa)	k (nm/s/Pa)
<u> (nm)	$\sqrt{\langle u^2 \rangle}$ (nm)				
2*	0.7	6.5	2.66	7.1	1.49
2*	1.5	10	2.66	7.1	1.62
2*	2	13	2.66	7.1	1.68
2*	4	20.5	2.66	7.1	1.77
11.42**	1.389	104	2.66	7.1	1.90
12.10**	1.389	110	2.66	7.1	1.90
22***	4	174	2.66	7.1	1.91

*<u> from TEM(Rodewald & Karnovsky, 1974) ** parameters from SEM(Gagliardini et al., 2010) *** parameters from helium ion microscopy (Rice et al., 2013).

When κ_{GBM} = 1.5 nm^2 (Deen et al., 2001) and <u> obtained from SEM (Gagliardini et al., 2010) or helium ion microscopy (Rice et al., 2013) is employed, the obtained hydraulic permeability is approximately 1.9 nm/s/Pa, which falls into the range estimated from human glomerular filtration rate (GFR) at 1.61-4.54 nm/s/Pa (Drumond & Deen, 1994). If κ_{GBM} is assumed to be 3 nm^2, k increases to 3 nm/s/Pa. The contribution of the epithelial cell layer to fluid restriction is negligible.

If, instead, u is assumed to follow the log-normal distribution with <u> = 2 nm, the total hydraulic permeability and the contribution of the epithelial cell layer depends on the standard deviation of u. If $\sqrt{\langle u^2 \rangle}$ = 0.7 nm, the contribution of the epithelial cell layer is significant (with k_{ep} slightly lower than k_{en}). The overall hydraulic permeability at 1.49 nm/s/Pa, however, is slightly lower than the range estimated from GFR. For higher values of $\sqrt{\langle u^2 \rangle}$ that yield the sieving coefficient closer to the sieving

coefficient of ficoll obtained from urinanalysis, the obtained hydraulic permeability at 1.62 - 1.77 nm/s/Pa falls into the range of hydraulic permeability estimated from GFR, whereas the contribution of the epithelial cell layer to fluid restriction is less than the other two layers.

จุฬาลงกรณ์มหาวิทยาลัย
Chulalongkorn University

Chapter 7
Discussion: Medical Implication

7.1 Contribution of type IV collagen and GAG to solute restriction in the GBM

As shown earlier in Figs. 3.1 and 3.2, the calculation of the diffusive permeability by including only the hydrodynamic interaction between solute and GAG yields the diffusive permeability that agrees well with an empirical expression obtained from ultrafiltration through an isolated GBM(Bolton et al., 1998) for small and medium-sized solute. In addition, it also gives the sieving coefficient that agrees well with experimental data from the experiment from the very same paper. The notion that, while type IV collagen provides tensile strength to the GBM, it does not contribute to size selectivity of the GBM (as much as GAGs) is supported by the fact that mutations in adult type IV collagen result in a GBM structure distortion and Alport syndrome where hematuria and only mild proteinuria are observed(Barker et al., 1990; Henry & Duling, 1999; Wartiovaara et al., 2004). Type IV collagen maintains the GBM structure, whereas GAGs contributes to restriction of solute passage.

จุฬาลงกรณ์มหาวิทยาลัย
Chulalongkorn University

7.2 Roles of the slit diaphragm and the GAG chains in the endothelial fenestrae in glomerular size-selectivity

Results shown in Figs. 7.1A and 7.1B are the sieving coefficient calculated by assuming that u follows the log-normal distribution with $\langle u \rangle$ = 12.10 nm (according to the SEM observation of Gagliardini et al. (2010)) and $\langle u \rangle$ = 22 nm (according to the observation of Rice et al. (2013) using the helium ion microscopy), whereas the sieving coefficient shown in Figs. 7.2A and 7.2B are calculated by assuming that $\langle u \rangle$ = 2 nm (according to the TEM observation of Rodewald and Karnovsky (1974) and the observation of Wartiovaara et al. (2004) from electron tomography). $\sqrt{\langle u^2 \rangle}$ is chosen at 2 nm and 4 nm as they yields the sieving coefficient that are close to sieving of ficolls from urinalysis in human. Two physiological variation is examined: the absence of the

slit diaphragm often observed in patients with nephrotic syndrome of Finnish type, and patients with epithelial podocyte effacement, and the additional absence of the GAG in the endothelial fenestrae.

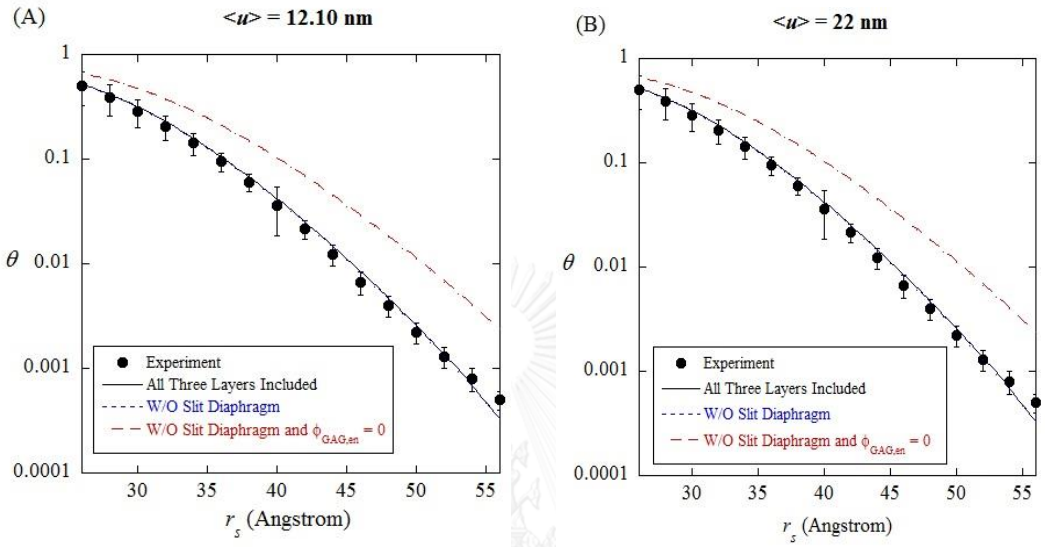

Figure 7.1: Sieving coefficient as a function of solute radii calculated by assuming that (A) <*u*> = 12.10 nm and (B) <*u*> = 22 nm. Results are shown for the case of all three layers included (solid lines), in absence of the epithelial slit (blue dashed lines), and in absence of both the epithelial slit and the GAG chains within the endothelial fenestrae (red dashed line). Also presented are sieving coefficient of ficoll obtained from urinalysis in human(Blouch et al., 1997).

All four figures exhibit a similar trend in absence of the slit diaphragm and GAG chains in the endothelial fenestrae, despite the difference in <*u*> employed. If <*u*> = 12.10 nm and 22 nm are assumed, the absence of the slit diaphragm from the glomerular capillary wall (achieved by setting θ_{ep}=1) causes the total sieving coefficient to increases very slightly (less than 1 %) for the entire range of solute radii presented. If <*u*> = 2 nm $\sqrt{\langle u^2 \rangle}$ = 2 nm are assumed, an increase in the total sieving coefficient due

to the loss of the slit diaphragm varies from approximately 9% for r_s = 2.6 nm to less than 1% for $r_s \geq 4.2$ nm. If, instead, <u> = 2 nm $\sqrt{\langle u^2 \rangle}$ = 4 nm are assumed, an increase in the sieving coefficient is even smaller ranging from 3 % for r_s = 2.6 nm to less than 1% for $r_s \geq 3.8$ nm. For results presented in all four figures, the increase of the sieving coefficient due to the absence of the slit diaphragm decreases as a function of solute radii. This indicates that the presence of the slit diaphragm affects transport of small solutes, but does not affect the passage of larger solutes, possibly because the larger solutes are already restricted by the GBM and the endothelial cell layer as will be discussed below.

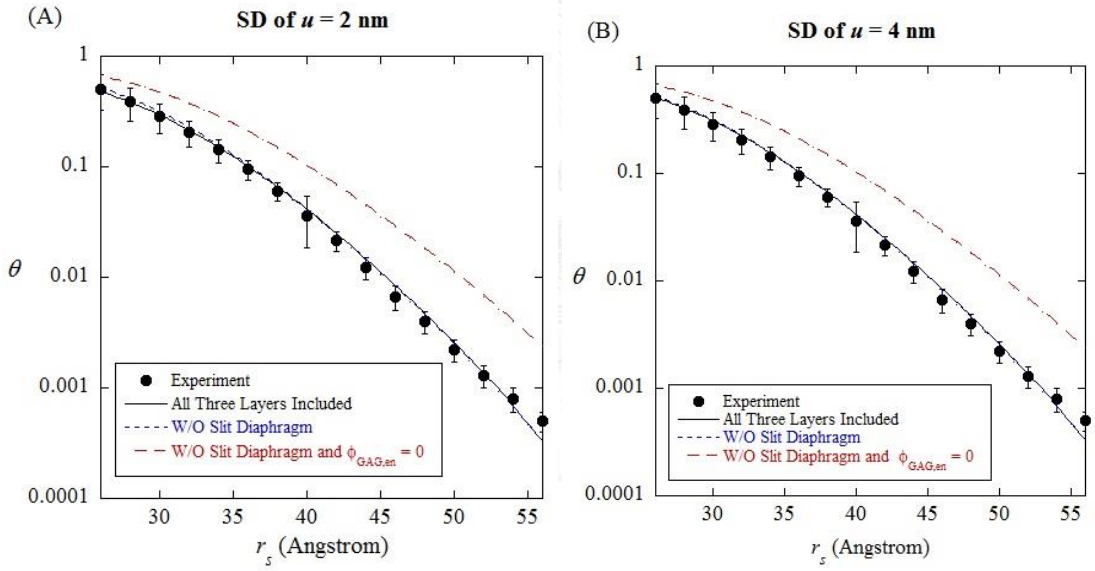

Figure 7.2: Sieving coefficient as a function of solute radii calculated by assuming that <u> = 2 nm with (A) $\sqrt{\langle u^2 \rangle}$ = 2 nm and (B) $\sqrt{\langle u^2 \rangle}$ = 4 nm. Results are shown for the case of all three layers included (solid lines), in absence of the epithelial slit (blue dashed lines), and in absence of both the epithelial slit and the GAG chains within the endothelial fenestrae (red dashed line). Also presented are sieving coefficient of ficoll obtained from urinalysis in human(Blouch et al., 1997).

The fact that the absence of the slit diaphragm does not cause a major change in the sieving coefficient of uncharged solutes seems to contradict with the observation of proteinuria in patients with the nephrotic syndrome of the Finnish type characterized by the loss of foot process and the slit diaphragm. However, it has also been observed that proteinuria can occur without losses of slit diaphragm or podocyte effacement. For instance, proteinuria is observed in patients with early-staged diabetes where the epithelial cell layer and the slit diaphragm are still intact. (The loss of the slit diaphragm is observed in patients with later-staged diabetes, but not in early-staged diabetes.)

The work presented here indicates that the endothelial cell layer also plays a significant role in glomerular solute restriction. As shown in Figs 7.1A - 7.2B, if the GAGs that fill the endothelial fenestrae disappear from the barrier, the glomerular sieving coefficient increases significantly. The percentage of the sieving coefficient increase grows rapidly as a function solute radii up to more than one order of magnitude for large solutes, indicating that the GAGs within the endothelial fenestrae is responsible for restricting large solutes. Whereas the direct study of the glomerular endothelial glycocalyx is not possible, a decrease in the systemic endothelial glycocalyx volume obtained from a tracer dilution technique has been associated with an increase in urinary protein excretion in patients with type 1 diabetes(Nieuwdorp et al., 2006; Satchell, 2013).

จุฬาลงกรณ์มหาวิทยาลัย
Chulalongkorn University

Our results indicate that glycoaminoglycan (GAGs) plays a crucial role due to its presence in both the GBM and the endothelial fenestrae. This is supported by experiments involving streptozotocin-induced diabetic rats exhibiting albuminuria, where the loss of GAGs in the glomerular barrier has been demonstrated(Satoha et al., 2010). Previous studies associated the role of GAGs with glomerular charge selectivity due to their negative charges. Our study, on the other hand, indicates that GAGs also contribute significantly to the size selectivity of the glomerular capillary wall. As aforementioned, exposures to GAG-degrading enzymes decreased the sieving coefficient of uncharged ficolls obtained from urinalysis and cool perfused isolated kidney experiments performed in rats(Jeansson & Haraldsson, 2003).

Chapter 8
Summary and Conclusion

In order to calculate the solute sieving coefficient through an epithelial cell layer, the slit diaphragm was modeled as a row of parallel fibers. The sieving coefficient through slit diaphragm through a row of parallel cylinders with uniform spacing had been determined from solving the steady-state convection diffusion equation(Drumond & Deen, 1995). However, an assumption of uniform fiber spacing cannot explain the more slowly declining of sieving coefficient from experimental data from *in vivo* urinalysis. In this work, the non-uniform spacing between adjacent fibers was assumed to follow the log-normal distribution with the parameters based on recent observations from scanning electron microscopy (SEM) and helium ion scanning microscopy.

Contribution to size selectivity and hydraulic permeability during glomerular filtration of the three cellular layers of the glomerular capillary wall was examined through a mathematical simulation. The GBM was modeled as an isotropic fibrous medium consisting majorly of two fibers: type IV collagen and glycoaminoglycan (GAG). The solute concentration through the GBM were determined by solving pseudo-steady convection-diffusion equation. A calculation employing a 1:1 mixture of GAG and type IV collagen led to the diffusive permeability that was very close to the empirical expression obtained from ultrafiltration through an isolated GBM if the enhanced drag and solute diffusivity was calculated by considering only GAG-solute interaction. This was due to a higher numbers of GAG presented in the GBM when assuming that the volume fraction of the GAG and collagen were equal at 0.05; only an interaction between GAG and macromolecules affect the reduction of the diffusivity and protein selectivity, whereas the role of type IV collagen was to maintain the GBM structural integrity. The same approach was employed in calculating the reduced diffusivity in the GAG-filled endothelial fenestrae.

Because the calculation of the change in convection rate of spheres suspended in random array of fibers was also currently not available, the convection rate of

spherical solutes transported through the GBM and the endothelial fenestrae, therefore, was obtained from assuming that the velocity of a sphere freely suspending in the GBM and in the fiber-filled fenestrae was that of a force-free sphere moving in Brinkman media with Darcy permeability equal to Darcy permeabilities of these two cellular layers. After the diffusivity and the changed convective rate were determined, the sieving coefficient through each layer was calculated from a solution of a steady-state convection diffusion equation.

The total sieving coefficient was obtained as the product of sieving coefficient through each layer. Even though the mean and standard deviation of spacing between adjacent fibers obtained from TEM, SEM, electron tomography and helium ion microscopy greatly differed, their difference did not affect the total sieving coefficient. The total sieving coefficient decreased when the volume fraction of GAG in endothelial fenestrae (ϕ_{GAG}^{en}) increased; the obtained total sieving coefficient agree with the sieving coefficient of ficoll from in vivo urinalysis in human when ϕ_{GAG}^{en} was set at 0.07. The sieving coefficient through GBM was the smallest among all three layers for the range of solute sizes presented in this work, indicating that it played a crucial role in solute restriction during glomerular filtration. Our results also indicated that glycocalyx-filled endothelial fenestrae affected both glomerular size-selectivity and charge-selectivity. Our results indicated that the absence of glycoaminoglycan (GAG) in the endothelial fenestrae caused a significant increases in the total sieving coefficient which increases as a function of solute radii. For large solute, this increase was more than one order of magnitude, implying that GAGs within the endothelial cell layer played a major role in restricting large solutes. The effect of the slit diaphragm seemed to be smaller than previously believed. An increase in sieving coefficient due to the slit diaphragm loss decreases as a function of solute radii, indicating that its presence is more crucial to restriction of smaller solutes than to that of larger solute.

In addition to obtaining the sieving coefficient that agreed well with the experimental data from urinalysis in human, the total hydraulic permeability from our calculation also fell into the range of hydraulic permeability estimated from human glomerular filtration rate (1.61-4.5 nm/s/Pa). Calculated results confirmed that the total

glomerular hydraulic permeability was affected by hydraulic permeability of the GBM and that of the endothelial fenestrae, whereas the fluid restriction of epithelial cell layer had a smaller effect.

The determination of total glomerular sieving coefficient in this thesis mainly focuses on size – selectivity of glomerular capillary wall. Charge on the glomerular sieving coefficient is not included in this research, and is one possible direction of our future work. Additional directions for future work includes the change in total sieving coefficient in nephrotic humans due to other physiological changes such as GBM thickness, width of structural unit and change in glomerular filtration rate.

จุฬาลงกรณ์มหาวิทยาลัย
Chulalongkorn University

REFERENCES

Amsden, B. (1998). Solute diffusion in hydrogels. An examination of the retardation effect. *Polymer Gels and Networks, 6*, 13-43.

Barker, D. F., Hostikka, S. L., Zhou, J., Chow, L. T., Oliphant, A. R., Gerken, S. C., et al. (1990). Identification of Mutations in the COL4A5 Collagen Gene in Alport Syndrome. *Science, New Series, 248*, 1224-1227.

Blouch, K., Deen, W. M., Fauvel, J.-P., Bialek, J., Derby, G., & Myers, B. D. (1997). Molecular configuration and glomerular size selectivity in healthy and nephrotic humans. *Am. J. Physiol, 273*(Renal Physiol. 42), F430 - F437.

Bolton, G. R., Deen, W. M., & Daniels, B. S. (1998). Assessment of the charge selectivity of glomerular basement membrane using Ficoll sulfate. *Am. J. Physiol, 274*((Renal Physiol. 43)), F889–F896.

Brady, J. F. (1994). *Hindered diffusion.* Paper presented at the American Institute of Chemical Engineers Annual Meeting, San Francisco, CA.

Clague, D. S., & Phillips, R. J. (1996). Hindered diffusion of spherical macromolecules through dilute fibrous media. *Phys. Fluids, 8*, 1720 –1731.

Curry, F. E., & Michel, C. C. (1980). A fiber matrix model of capillary permeabilty. *Microvasc. Res., 20*, 96-99.

Deen, W. M., Bridges, C. R., Brenner, B. M., & Myers, B. D. (1985). Heteroporous model of glomerular size selectivity: application to normal and nephrotic humans.
Am. J. Physiol., 249(Renal Fluid Electrolyte Physiol. 18), F374-F389.

Deen, W. M., Lazzara, M. J., & Myers, B. D. (2001). Structural determinants of glomerular permeability. *Am J Physiol Renal Physiol, 281*(OCTOBER 2001), 579-596.

Drumond, M. C., & Deen, W. M. (1994). Stokes Flow Through a Row of Cylinders Between Parallel Walls: Model for the Glomerular Slit Diaphragm. *Journal of Biomechanical Engineering, 116*(May 1994), 184-189.

Drumond, M. C., & Deen, W. M. (1995). Hindered Transport of Macromolecules Through a Single Row of Cylinders: Application to Glomerular Filtration. *Journal of Biomechanical Engineering, 117*(November 1995), 414-422.

Edwards, A., Daniels, B. S., & Deen, W. M. (1997). Hindered Transport of Macromolecules in Isolated Glomeruli.II. Convection and Pressure Effects in Basement Membrane. *Biophysical Journal, 72*(January 1997), 214-222.

Edwards, A., Daniels, B. S., & Deen, W. M. (1999). Ultrastructural model for size selectivity in glomerular filtration. *Am J Physiol Renal Physiol, 276*(Renal Physiol. 45), F892-F902.

Gagliardini, E., Conti, S., Benigni, A., Remuzzi, G., & Remuzzi, A. (2010). Imaging of the Porous Ultrastructure of the Glomerular Epithelial Filtration Slit. *J Am Soc Nephrol, 21*, 2081–2089.

Haraldsson, B., Nystrom, J., & Deen, W. M. (2008). Properties of the Glomerular Barrier and Mechanisms of Proteinuria. *Physiological Reviews, 88*(April 2008), 451 - 487.

Henry, C. B. S., & Duling, B. R. (1999). Permeation of the luminal capillary glycocalyx is determined by hyaluronan. *Am J Physiol Heart Circ Physiol, 277*, H508-H514.

Hora, K., Ohno, S., Oguchi, H., Furukawa, T., & Furuta, S. (1990). Three-Dimensional Study of Glomerular Slit Diaphragm by Quick-Freezing and Deep-Etching Replica Method. *Eur. J. Cell Biol, 53*, 402-406.

Jeansson, M., & Haraldsson, B. (2003). Glomerular Size and Charge Selectivity in the Mouse after Exposure to Glucosaminoglycan-Degrading Enzymes. *J Am Soc Nephrol, 14*, 1756–1765.

Karl Tryggvason, & Jorma Wartiovaara. (2005). How Does the Kidney Filter Plasma? *PHYSIOLOGY, 20*(April 2005), 96-101.

Layton, A. T., & Edwards, A. (2014). *Mathematical Modeling in Renal Physiology*: Springer.

Mattern, K. J. (2008). *Permeability Studies in Biomimetic Glycosaminoglycan-Hydrogel Membranes.* (DOCTOR OF PHILOSOPHY IN CHEMICAL ENGINEERING), MASSACHUSETTS INSTITUTE OF TECHNOLOGY.

Nieuwdorp, M., Mooij, H. L., Kroon, J., Atasever, B., Spaan, J. A. E., Ince, C., et al. (2006). Endothelial Glycocalyx Damage Coincides With Microalbuminuria in Type 1 Diabetes. *DIABETES, 55*(APRIL 2006), 1127-1132.

Öberg, C. M., & Rippe, B. (2014). A distributed two-pore model: theoretical implications and practical application to the glomerular sieving of Ficoll. *Am J Physiol Renal Physiol, 306*, F844–F854.

Ohlson, M., Sorensson, J., Lindstrom, K., Blom, A. M., Fries, E., & Haraldsson, B. (2001). Effects of filtration rate on the glomerular barrier and clearance of four differently shaped molecules. *Am J Physiol Renal Physiol, 281*, F103–F113.

Phillips, R. J. (2000). A Hydrodynamic Model for Hindered Diffusion of Proteins and Micelles in Hydrogels. *Biophysical Journal, 79*(December 2000), 3350–3354.

Rice, W. L., Hoek, A. N. V., Paunescu, T. G., Huynh, C., Goetze, B., Singh, B., et al. (2013). High Resolution Helium Ion Scanning Microscopy of the Rat Kidney. *PLOS ONE, 8*(3), e57051(57051-57059).

Rodewald, R., & Karnovsky, M. J. (1974). Porous Substructure of the Glomerular Slit Diaphragm in the Rat and Mouse. *The Journal of Cell Biology, 60*, 423-433.

Sangani, A. S., & Acrivos, A. (1982). Slow Flow Past Periodic Arrays of Cylinders with Application to Heat Transfer. *Int. J. Multiphase Flow, 8*, 193-206.

Satchell, S. (2013). The role of the glomerular endothelium in albumin handling. *S. Nat. Rev. Nephrol., 9*, 717–725.

Satoha, T., Katoa, H., Kumagaia, Y., Yoneyamab, M., Satoa, S., Matsushitaa, K., et al. (2010). LGP2 is a positive regulator of RIG-I– and MDA5-mediated antiviral responses. *PNAS, 107*, 1512–1517.

Wartiovaara, J., Öfverstedt, L.-G., Khoshnoodi, J., Zhang, J., Mäkelä, E., Sandin, S., et al. (2004). Nephrin strands contribute to a porous slit diaphragm scaffold as revealed by electron tomography. *The Journal of Clinical Investigation, 10*(November 2004), 1475-1483.

APPENDIX

จุฬาลงกรณ์มหาวิทยาลัย
Chulalongkorn University

Determination of *g(u)* of a row of parallel cylinders with non-uniform spacing using the Newton-Raphson method

The relationship between hydraulic permeability, dimensionless flow resistance and the distribution, $g(u)$, is as following

$$< k_s > - \frac{\int_0^\infty (u+R)^2 \, f_T^{-1} g(u) du}{\eta \int_0^\infty (u+R) g(u) du} = 0 \qquad \text{(A1)}$$

If the dimensionless flow resistance is known and $g(u)$ follows a gamma distribution, for a given value of γ_1 , γ_2 can be calculated from the averaged hydraulic permeability through the slit diaphragm, $<k_s>$, by solving equation (A1) using the Newton-Raphson method, a very well-known numerical method employed in finding successively better approximation of the root of the equation. The Newton-Raphson scheme was written using MATLAB v. 2011b software (Mathwork, Netick, MA, USA). Once γ_1 and γ_2 are obtained, the gamma distribution function of the gap half-width is known, and the mean and standard deviation of u can then be calculated from equation (6.7a) and the square root of the solution of equation (6.7b). A similar procedure can be applied to determine the parameters of $g(u)$ if $g(u)$ follows a log-normal distribution.

Results obtained from this numerical scheme are shown below in Figs. (A1) and (A2) where values of γ_2 and the mean value of fiber gap half-width, $<u>$, are plotted as a function of numbers of iterations, respectively. The results are shown for $<k_s>$ = 114 nm/s/Pa. The epithelial slit fiber radius, R, is estimated from images from electron tomography and assumed to be 4.5 nm. As shown in the figures, convergence of the Newton-Raphson method is achieved after a few iterations, reaching the same values of the mean and standard deviation of fiber spacing of the epithelial slit regardless of the initial guess for γ_2, denoted below in the figures as γ_{20}. For γ_{20} = 2, 3, 4, 7, 8, and 9 nm^{-1}, the final solution for γ_2 is always 5.40 nm^{-1} for as illustrated in Figure (A1),

always yielding the mean value of the half-width of gap between adjacent fibers in the epithelial slit, <*u*>, at 2.06 nm as shown in Figure (A2).

In addition, the standard deviation of the gap half-width can also be obtained from substituting γ_1 and γ_2 calculated using the Newton-Raphson method shown in Figure (A1) into Eq. (6.7b). The result is shown in Fig. (A3) where the standard deviation of *u* is plotted as a function of the number of iterations. Regardless of the initial guess for γ_2 , the standard deviation of *u* always converge to 0.62 nm.

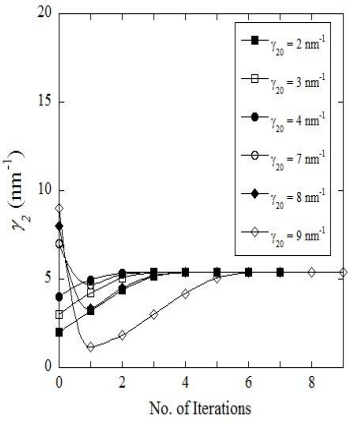

Figure A1: the parameter γ_2 of the gamma distribution (as shown in equation (6.5)) as a function of number of iterations. γ_{20} are initial guesses for γ_2 . γ_1 = 11.11. <k_s> = 114 nm/s/Pa at 37˚C.

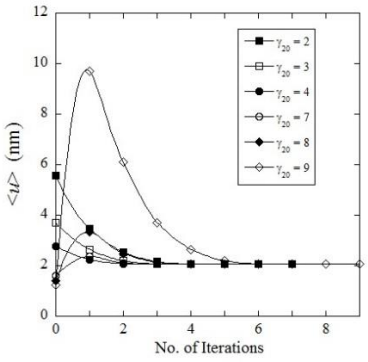

Figure A2: <*u*>, the mean value of the fiber spacing half-width, as a function of number of iterations. γ_{20} is the initial guess for γ_2 . γ_1 = 11.1. <k_s> =114 nm/s/Pa at 37˚C.

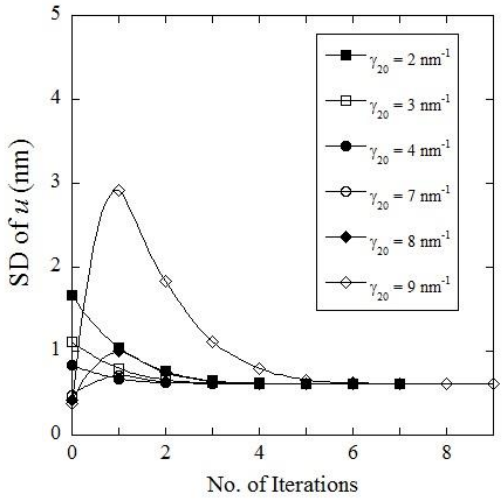

Figure A3: the standard deviation of the half-width of the gap between adjacent fibers of the slit diaphragm as a function of number of iterations. γ_{20} is the initial guess for γ_2. γ_1 = 11.1. <k_s> =114 nm/s/Pa at 37˚C.

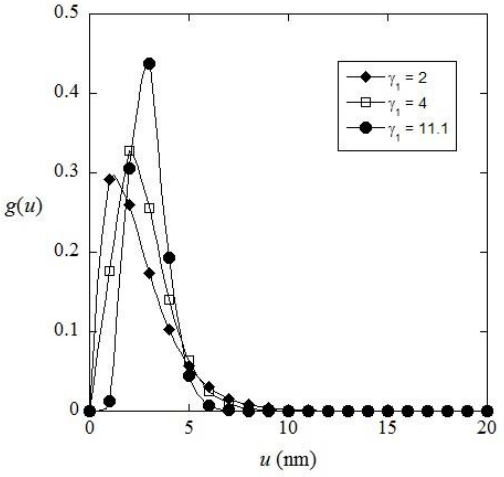

Figure A4: Distribution function, *g(u)*, of the half-width of the gap between adjacent fibers of the slit diaphragm as a function of u. γ_1 = 2, 4 and 11.1. <k_s> = 114 nm/s/Pa at 37˚C.

For a given value of γ_1, the Newton-Raphson method yields a value of γ_2 that gives the desired value of $<k_s>$. Shown in Fig. (A4) is the distribution, $g(u)$, that yields k_s at 114 nm/s/Pa for γ_1 = 2, 4 and 11.1. For different values of γ_1, the obtained γ_2 and $g(u)$ are different, resulting in different values of the mean and standard deviations of u as shown in the figure.

For each value of γ_1, there is a value of γ_2 that yield the appropriate value of $<k_s>$. In order to determine which pair of γ_1 and γ_2 to be employed, we need to know the solutes sieving coefficient. The appropriate γ_1 and γ_2 have to yield both appropriate values of hydraulic permeability as well as solute sieving as a function of solute sizes.

จุฬาลงกรณ์มหาวิทยาลัย
Chulalongkorn University

VITA

Mr. Numpong Punyaratabandhu was born on October 30, 1991 in Lampang, Thailand. He received the bachelor degree (1st class honors) from the Department of Physics, Faculty of Science, Chulalongkorn University in 2013. He was admitted to the master's degree Program of Physics, Faculty of Science, Chulalongkorn University and completed the program in 2015.

Proceeding Publication:

2016 N. Punyaratabandhu and P. Dechadilok. Determination of the Distribution Function of Spacing between Fibers of a Row of Parallel Cylindrical Fibers with Non-Uniform Spacing from its Hydraulic Permeability: Applications to Glomerular Filtration. Siam Physics Congress 2016. Ubon Ratchathani, Thailand(June 8 – 10, 2016)

Conference presentation:

1) N. Punyaratabandhu and P. Dechadilok. Transport of Macromolecules through Glomerular Capillary Wall. Siam Physics Congress 2015. Krabi, Thailand: 20 – 22 May 2015

2) N. Punyaratabandhu and P. Dechadilok. Transport of Macromolecules through Glomerular Capillary Wall. The 20th Biological Science Graduate Congress. Bangkok, Thailand: 9 - 11 December 2015

3) N. Punyaratabandhu and P. Dechadilok. Filtration of Electrically Neutral Macromolecules through Glomerular Capillary Wall. Siam Physics Congress 2016. Ubon Ratchathani, Thailand: 8 – 10 June 2016